Failure Prediction of Adhesively Bonded Hardboard Door Skin Joints

by

Bryan Christopher Mosher

Thesis submitted to the Faculty of Virginia Polytechnic Institute and State University in partial fulfillment of the requirements for the degree of

Master of Science

In

Engineering Mechanics

S. Thangjitham, Co-Chair

J. Loferski, Co-Chair

N. Dowling

May 19, 2005
Blacksburg, Virginia

Keywords: Hardboard, Wood Composite, Wood, Finite Element, Beam, Elastic Foundation, Failure, Adhesive

FAILURE ANALYSIS OF ADHESIVELY BONDED HARDBOARD DOOR SKIN JOINTS

by

Bryan Christopher Mosher

(ABSTRACT)

Wood and wood based composites such as hardboard have become very common materials for use in non-structural applications, which include pre-finished paneling, siding, exterior trim, furniture, and door skins. This thesis describes the results of a study of the failure of hardboard door skins. Forces applied during manufacture load the door skins in bending, and in some cases cause a split at the edge of the hardboard. A finite element model as well as a closed form solution based on mechanics of materials were developed to analyze the stresses and deformations of the door skin/stile assembly so that stresses could be predicted for various stile widths and loading conditions. The wood members that make up the frame along the perimeter of the doors, or stiles, were modeled as orthotropic and their properties were selected from available literature. The hardboard was modeled as transversely isotropic, and its properties were determined experimentally. The closed form solution developed can be used to determine the critical geometry for different combinations of hardboard thickness and adhesive joint stiffness. It predicts that as the stile width decreases, the point of maximum deflection, and greatest stresses, moves toward the outside edge of the panel. The ability to predict the critical stile width, or the stile width below which the maximum deflection and stress occurs at the outside edge of the panel, allows one to design the joint to be able to withstand specific loadings and prevent unwanted delamination of the hardboard during manufacture.

Acknowledgements

First, I would like to thank Dr. Thangjitham and Dr. Loferski for all their guidance and help throughout my time as an M.S. student. I love to learn new things and I learned much about wood and engineering mechanics from you both. I also had a great time working with you both!

I would like to thank Dr. Dowling for serving on my committee, your commitment to teaching, and everything I learned from you about engineering mechanics and being a better teaching assistant.

I would like to thank Mike Hoffman of CMI Inc. for supplying materials and information on the hardboard product.

I would like to thank Bob Simonds and Rick Caudill. Ya'll were an enormous help in learning how to run experiments and work in a laboratory setting, especially since I had to teach it!

I would like to thank my parents for everything. Without ya'll, I would never have even had the opportunity to go to college, much less earn a Masters degree! Thank you for your provision, love and support throughout all of my schooling and of course for my whole life.

To my church family here in Blacksburg: ya'll are some of the best friends I have ever had. I have learned a lot from your examples of how to be worshippers of the Lord. I am going to miss you very much.

I am delighted to express my love and gratitude to my wife, Sarah, who has stood beside me, cheering me on and supporting me during the past two years.

Last and most importantly, I thank my God and Savior. Thank you for the talents and abilities You have blessed me with. Thank you Jesus for your gift; without You life would be meaningless.

Soli Deo Gloria

Bryan Mosher

Table of Contents

List of Figures

List of Tables

Chapter 1: Introduction

Wood and wood based composites have become very common materials for use in structural and non-structural applications. Popular panel materials include plywood, oriented strand board, particle board, medium density fiberboard, and hardboard. Hardboard, the material studied in this thesis, has many common uses, which include pre-finished paneling, siding, exterior trim, furniture, and door skins. "Hardboard is a composite panel manufactured primarily from interfelted lingo-cellulosic fibers consolidated under heat and pressure" [5]. It is a non-structural material that is used primarily for decorative applications. This thesis describes the results of a study of the failure of hardboard door skins used to produce hollow-core doors for home interior use. The door skins are purchased from a hardboard manufacturer, and then glued onto wooden stiles that form the interior frame of the door. The stiles are rectangular pieces of wood approximately $1^1/_8$ in. × $1^1/_8$ in. × 7 ft., or the height of the door. Once the glue has dried, the doors are moved along a drive chain system on which they are trimmed to finish width. A "book trim" of $^3/_{16}$ in. is cut off each side of the door to bring it to finished width. As the door moves along the drive chain, hold down wheels secure the assembled door as it is trimmed to finish width as shown in Figure 1. The forces applied by the hold-down wheels load the door skin in bending, and in some cases causes the hardboard to split open at the edge of the door. A typical failure occurs at the outer edge of the loaded door skin where it is glued to the stile, and appears as a separation in the thickness of the hardboard. As mentioned, a "book trim" of $^3/_{16}$ in. is supposed to be cut off of each side of the door. However, the doors are not always assembled properly and the initial spacing between the stiles varies, and in some cases the stiles are not parallel to

each other. These assembly errors result in varying final stile widths from the trimming process, and when the stiles are trimmed down to below a critical value, the hardboard splitting failure usually occurs and the door is rejected as a manufacturing defect. This splitting failure is shown in Figure 2.

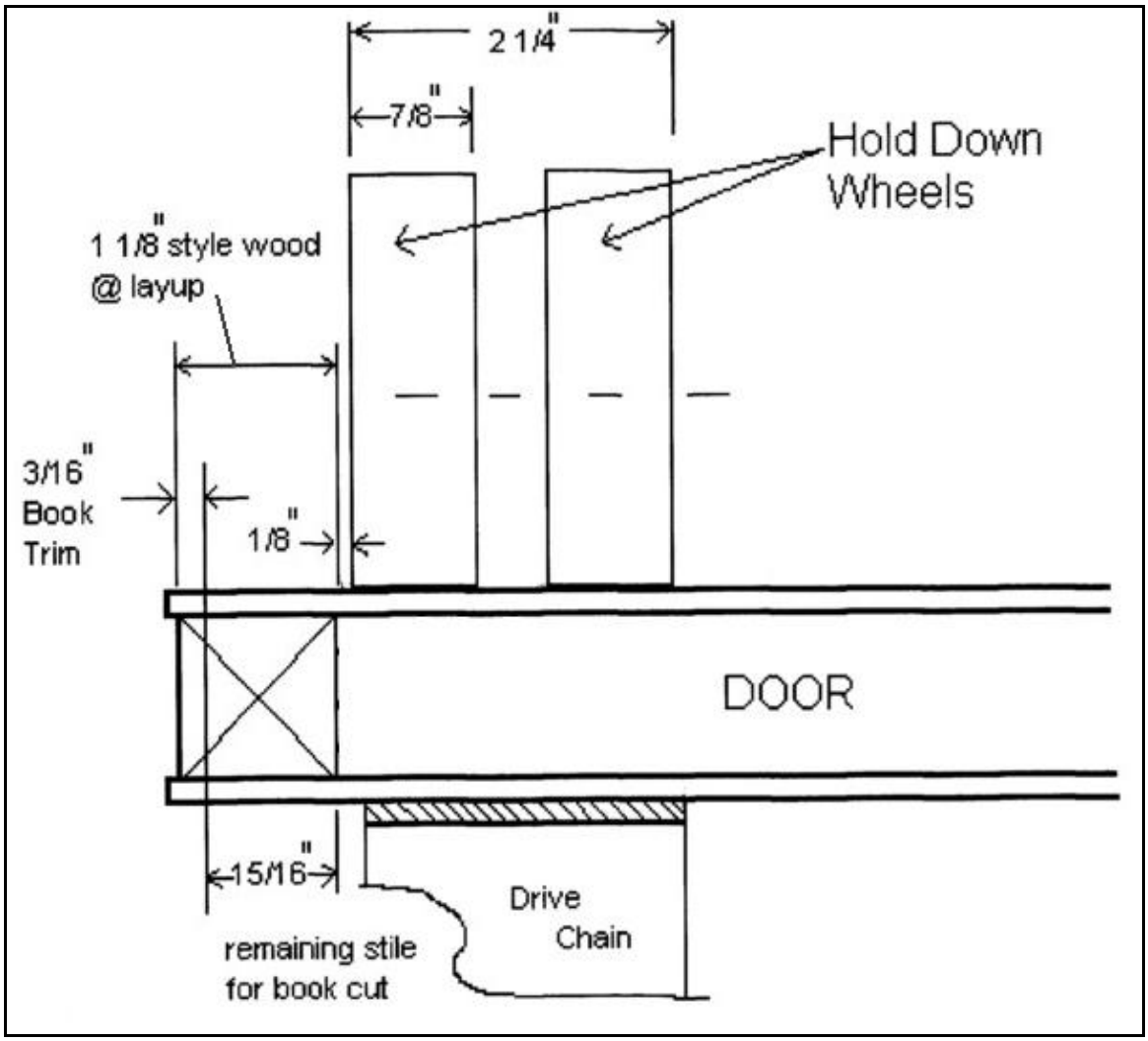

Figure 1: Door Manufacturing Process Geometry

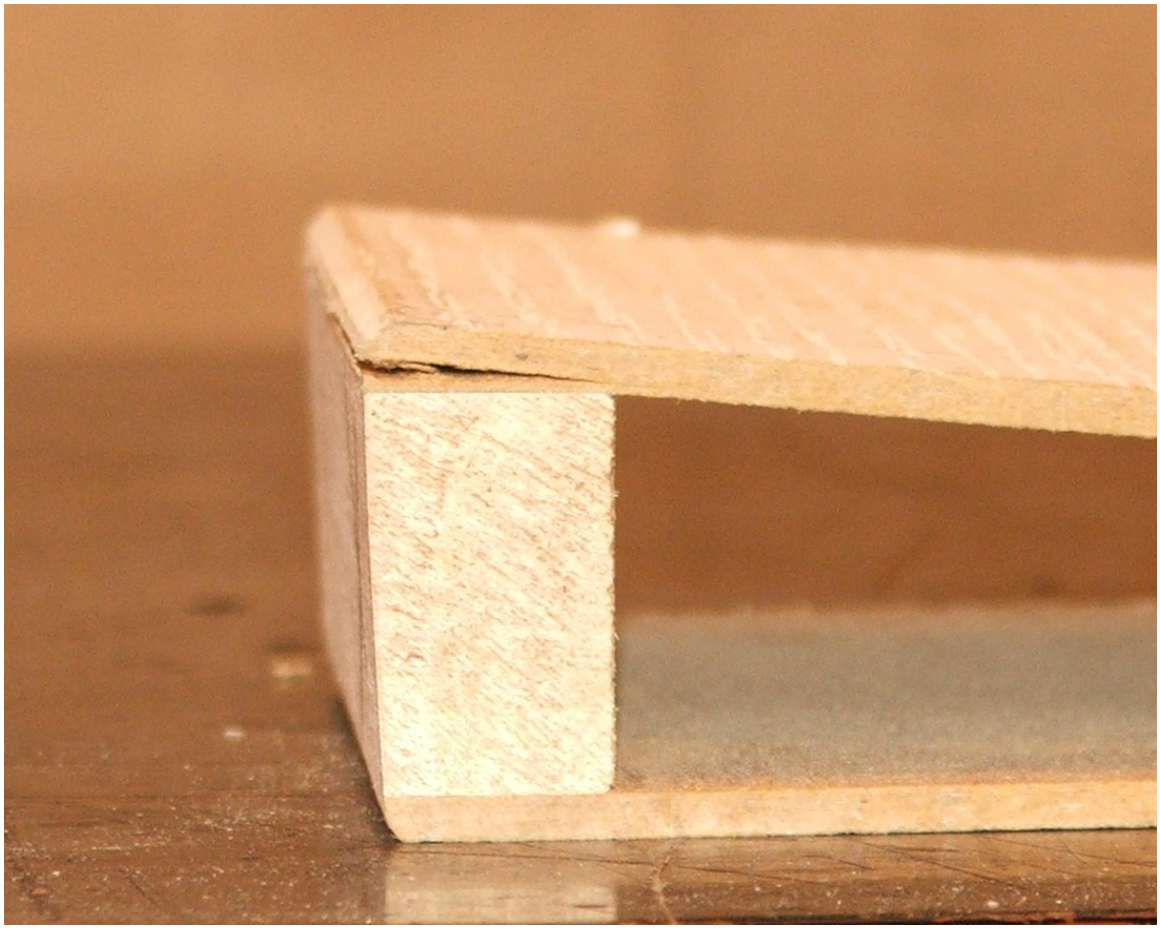

Figure 2: Hardboard Splitting Failure

The objectives of this project were to experimentally determine the engineering properties of the hardboard, develop an engineering model to analyze the stresses and deformations of the door skin/stile assembly, experimentally validate the engineering model, and predict stile widths that will minimize the formation of critical crack producing stresses.

Two fundamental mathematical models were developed: (1) a finite element analysis (FEA) model of the wood door stile and hardboard door skin, and (2) a closed form solution to the problem using concepts of mechanics of materials to analyze beams on elastic foundations, where the beam is the hardboard and the elastic foundation is the glue/stile interface. Engineering properties of the hardboard were measured to produce a transversely isotropic material model and material properties of the stiles were selected from available literature. These properties were used as input parameters in the FEA and closed form solution models.

Chapter 2: Literature Review

For several millennia, humans have employed wood as a major construction material. From the reconstruction of the Temple by King Solomon in Jerusalem in ancient Israel which imported "fine cedars of Lebanon" to the contemporary American dream house constructed with pine, wood has certainly proved its structural merit over time. By nature, wood is a heterogeneous material with regular discontinuities in which properties vary not only among species and within species, but also within individual trees.

The nature of wood and its properties can be modeled on many different levels, from the microscopic such as cells to the gross behavior of structural timbers. For engineering analysis, many assumptions are made for analytical convenience. Wood is commonly assumed to behave as an elastic material with well-defined directional dependence of its physical structure and mechanical properties. Of great importance with wood is the effect that factors such as density, grain orientation, defects, moisture content, and temperature have on its mechanical properties. Properties such as strength and modulus of elasticity (MOE) are directly proportional to the density. For grain orientation, or the angle between the grain direction and the long axis of the board, a rapid decrease in the MOE occurs as the angle increases from 0 to 45 degrees, with very little decrease after that. Defects such as knots and splits control the strength of structural lumber as they are the "weak link" and are unavoidable. The strength of wood is inversely proportional to the moisture content up to the fiber saturation point (FSP). The fiber saturation point is defined as the point in which only water bound in the cell walls remains.

For engineering analysis, wood can be modeled as an orthotropic material, either rectilinearly or cylindrically. For cylindrical modeling, longitudinal (L), radial (R), and transverse (T) directions are defined, and these directions are along the axis of growth, outward from the center or pith of the tree, and tangent to the growth rings respectively. Depending upon how a particular piece of lumber is cut, a transversely isotropic model can be used which neglects the differences between the radial and transverse directions. Wood in comparison to metals is not as strong or as stiff, but is much less dense (specific gravities around 0.5). The modulus of elasticity of steel is 29×10^6 psi where a typical value of wood along the grain (or growth direction) would be 1.6×10^6 psi. Values perpendicular to the grain are more than a factor of 10 less than that.

It is not possible to produce large panels out of solid sawn lumber, as trees 4 feet in diameter are scarce and unavailable for harvesting. The timber used for structural lumber as well as wood composite materials today is taken primarily from young plantation grown trees. Hence, other methods must be used to produce panels such as gluing small pieces or flakes of wood together (such as OSB) or cutting thin veneers from tress and gluing them together to produce plywood. Hardboard only requires wood fibers, and this allows the use of small diameter trees that have many defects such as knots and splits. The defects can be removed and the remaining material reduced down to fiber size. These fibers can then be collected, and pressed into any shape or size desired.

The ability to be pressed into the size or shape desired allows hardboard to be used in a variety of applications such as pre-finished paneling, siding, furniture, and door skins. All of these are non-structural applications however, and the material is not

inherently intended for structural use. As a result, information regarding the use of hardboard as an engineering material is very limited.

ANSI A135.4-2004 covers the standardization of material properties and characteristics for hardboard. Surface finish, dimensional tolerances, moisture content, thickness swelling, and water absorption requirements are presented as well as minimum values for the modulus of rupture and tensile strengths parallel and perpendicular to the panel surface. Hardboard is classified based on the physical properties shown in Table 1.

Examining the strengths in the last three columns, large differences in these properties for the different classes can be seen. Other properties needed such as the moduli of elasticity are not standardized, hence expected values are unknown. Material testing for the properties in Table 1 according to ASTM D1037 has been done and presented in the literature by a few authors including Biblis [2], and Superfesky and Lewis [13]. Research has also been done on the effects of processing and manufacturing including steam treatment and fiber acetylation as presented by Chow [4]. All of these tests however only include those properties addressed in the ANSI standard and ASTM D1037. Values such as Poisson's ratio and the out of plane modulus of elasticity were not considered.

Table 1: Hardboard Classifications (Source: Composite Panel Association [5])

Class	Nominal thickness	Water resistance (max. average per panel)		Modulus of rupture (min. average per panel)	Tensile strength (min. average per panel)	
		Water absorption based on weight	Thickness Swelling		Parallel to surface	Perpendicular to surface
	mm inch	percent	percent	MPa psi	MPa psi	MPa psi
	2.1 1/12	30	25			
	2.5 1/10	25	20			
1	3.2 1/8	25	20			
Tempered	4.8 3/16	25	20	41.4 6000	20.7 3000	0.90 130
	6.4 1/4	20	15			
	7.9 5/16	15	10			
	9.5 3/8	10	9			
	2.1 1/12	40	30			
	2.5 1/10	35	25			
2	3.2 1/8	35	25			
Standard	4.8 3/16	35	25	31.0 4500	15.2 2200	0.62 90
	6.4 1/4	25	20			
	7.9 5/16	20	15			
	9.5 3/8	15	10			
	3.2 1/8	35	30			
3	4.8 3/16	30	30			
Service-Tempered	6.4 1/4	30	25	31.0 4500	13.8 2000	0.52 75
	9.5 3/8	20	15			
	3.2 1/8	45	35			
	4.8 3/16	40	35			
4	6.4 1/4	40	30			
Service	9.5 3/8	35	25	20.7 3000	10.3 1500	0.34 50
	11.1 7/16	35	25			
	12.7 1/2	30	20			
	15.9 5/8	25	20			
	6.4 1/4	50	30			
5	9.5 3/8	40	25			
Industrialite	11.1 7/16	40	25	13.8 2000	6.9 1000	0.17 25
	12.7 1/2	35	25			
	15.9 5/8	30	20			

A complete engineering material model was need for finite element analysis. Wood is traditionally modeled as a cylindrically orthotropic material. Hardboard however does not have this cylindrical structure, and would be assumed to be rectilinearly orthotropic. Superfesky and Lewis [13] tested three medium-density hardboards and found that the resulting material properties did not differ significantly in the parallel and perpendicular directions in the plane of the panel. Such a result is reasonable as there is no specific fiber alignment during manufacture. This leads to the assumption that hardboard can be modeled as transversely isotropic. This reduced the testing required to obtain the needed material constants. Biblis [2] tested hardboard from 6 different manufacturers and found that "Certain board properties from some manufacturers are two times as strong as boards from other manufacturers." Hence, complete testing of material constants and strengths was done for the specific hardboard studied in this project.

Research on the performance of glued wood joints has been done in multiple contexts, from fracture mechanics to applications such as the joining of furniture elements. In the context of furniture assembly, Smardzewski [11] studied the effects of the heterogeneity of the glue bond, gas cavities, faulty glue bonds, and glue outflows. From a fracture perspective, a comparative review of fracture of wood composites and wood-adhesive joints was recently done by Conrad, Smith, and Fernlund [8]. Their review covered common geometries for structural bonded joints, the effects of the adherend or resin used to hold the product together, and the bondline thickness. Common geometries for structural bonded joints are shown in Figure 3.

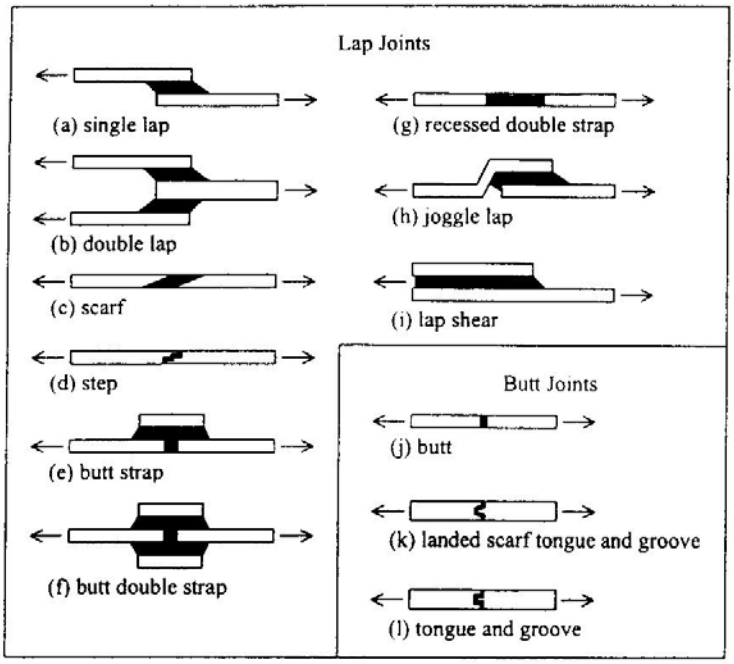

Figure 3: Common Structural Bonded Joints (Source: Conrad et al. [8][1])

Conrad et al. point out that the surfaces of the members being joined will affect the failure of a wood-adhesive joint; especially the path the crack propagates along. Three possible types of failure can occur: the crack can propagate in the wood or wood composite material alone, the adhesive alone, or at the wood adhesive interface. They cite a study that showed hand sanding the surfaces resulted in higher fracture toughness than machine sanded surfaces. The machine sanding was done in only one direction, whereas hand sanding was done in a back-and-forth motion. "The back-and-forth motion of the hand sanding leads to the creation of pre-failed interfaces between fibers. These planes of weakness allow the crack to deviate from the adhesive layer and arrest the crack, thus increasing the fracture toughness" [8]. Hence, in the formation of wood-adhesive joints, the surface preparation can affect the quality of the joint. Overall, they concluded that fracture mechanics is applicable to wood composites (such as hardboard)

[1] This figure is reproduced with the permission of Wood and Fiber Science from Volume 36, No. 1, pp. 26-39, 2004 of that journal

and, “All-wood component sizes: lumber, veneer, strands, particles, and fibers have been studied; and the majority of researchers have concluded that fracture of wood-adhesive joints should occur in wood alone and not at the wood-resin interface for optimum performance” [8].

Factors such as those studied by Smardzewski [11] could possibly have contributed to the behavior of the failure investigated, however the vast majority of failures in manufacturing were caused by the splitting of the hardboard, not the failure of the glue line. A layer of the hardboard material remained adhered to the stile after failure. In this case, the glue was “stronger” than the hardboard, and was not the “weak link” that caused failure. This corresponds with optimum failure as determined by Conrad, Smith and Fernlund [8].

Chapter 3: Experimental Work

3.1 Door Skin Material Testing

Material properties such as stiffness and strength are needed to predict the behavior of materials in response to forces and deformations. To develop an engineering material model of the hardboard, three tests were conducted: static bend, internal bond, and tension tests. The hardboard was modeled as transversely isotropic, which is a special case of the class of anisotropic materials (different properties in different directions). Transversely isotropic materials have the same properties in one plane and different properties in directions perpendicular to that plane. An *x-y-z* coordinate system was used to define the material directions as shown in Figure 4. The *x* and *z* directions are in the plane of the panel and the *y* direction is perpendicular to the *x-z* plane.

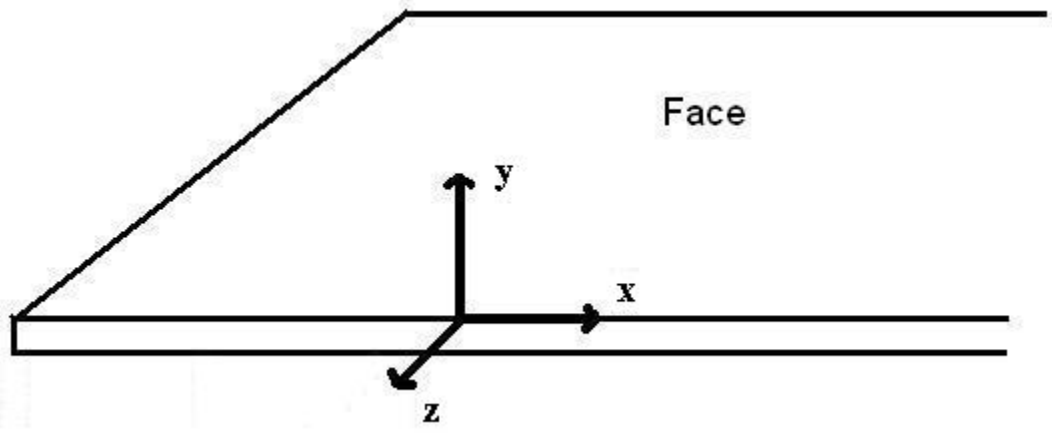

Figure 4: Hardboard Material Directions

The properties needed in the analysis were the elastic moduli (E_x, E_y, E_z), the Poisson's ratios (ν_{xy}, ν_{yz}, ν_{xz}, ν_{yx}, ν_{zy}, ν_{zx}), and the shear moduli (G_{xy}, G_{yz}, G_{xz}). The assumption of transverse isotropy yields $E_x = E_z$ and $G_{xy} = G_{yz}$, and

$$G_{xz} = \frac{E_x}{2 \cdot (1 + \nu_{xz})}$$

The lack of specific wood fiber alignment in the *x-z* plane during manufacture of the hardboard material permits these assumptions and greatly reduces the number of tests needed. The reciprocity relationships $\frac{E_A}{\nu_{AB}} = \frac{E_B}{\nu_{BA}}$ where A and B represent any of the directions *x, y,* or *z* ($A \neq B$) allow the determination of three of the Poisson's ratios when the other three and the elastic moduli are known. The shear moduli G_{xy} and G_{yz} were approximated by multiplying E_x by 0.08. The value of $0.08E_x$ is approximately the same ratio given in the "Wood Handbook" published by the USDA's Forest Products Laboratory for the quantity (G_{LT} /E_L) of Loblolly Pine [9]. Physical testing for these values would be very difficult, and was not attempted. Approximating this value using the same ratio as Pine is a reasonable assumption due to the wood fiber structure of the hardboard and is the most feasible method of obtaining the value.

3.1.1 Static Bend Tests

Static bending tests were conducted following the ASTM D1037 standard. The results were used to determine the elastic modulus E_x and the modulus of rupture (*MOR*, or *R*) which is the maximum bending stress at failure. Ten specimens were randomly cut out of the sample materials provided by the manufacturer with dimensions L = 3.0 in, b = 2.0 in, and d = 0.135 in. An MTS 10/GL universal testing machine equipped with a 200 lb load cell was used to load the specimens in three-point bending (Figure 5).

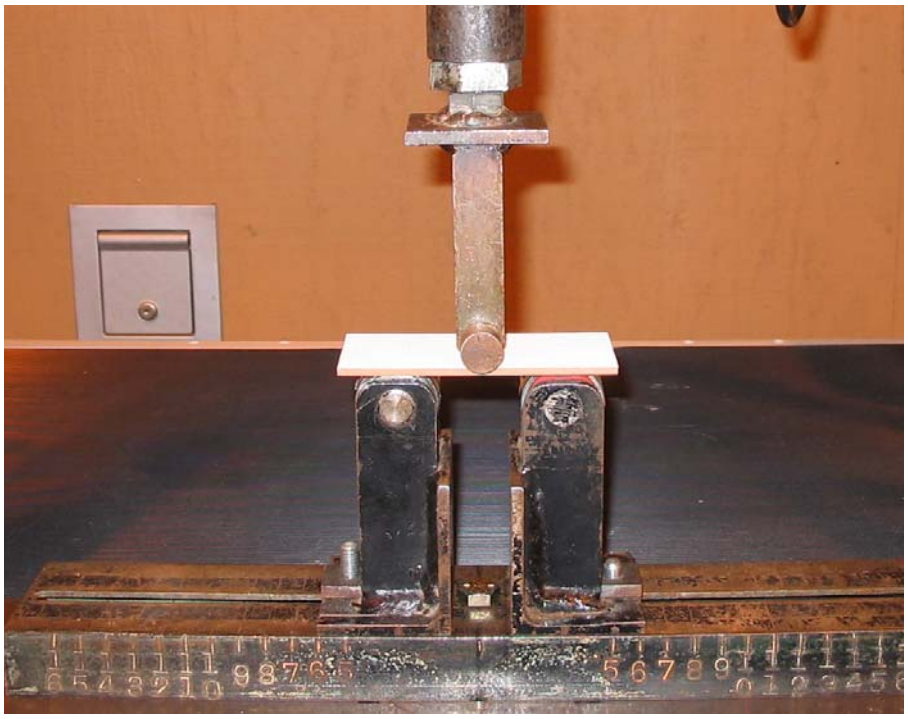

Figure 5: Static Bend Test Setup

Load and deflection were recorded until failure of the specimen. The linear region of the load versus deflection curve was used to compute the modulus, E_x, and the maximum load was used to compute the modulus of rupture. A typical load versus deflection curve for the bend tests is shown in Figure 6.

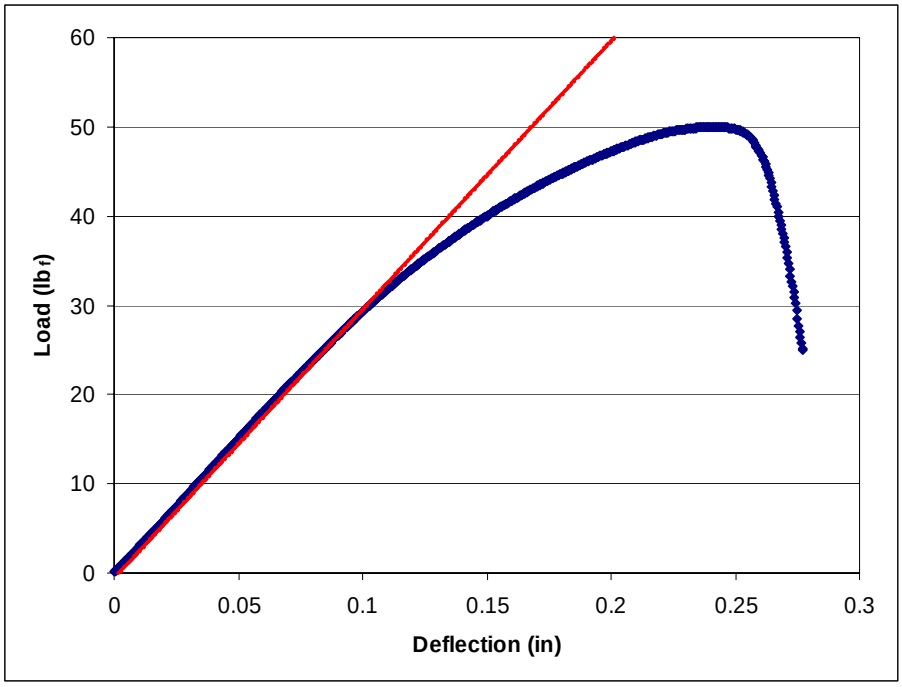

Figure 6: Load Versus Deflection for 3 Point Bend Tests

The modulus E_x was computed from linear beam theory, using the known relationship between the mid-span deflection and applied load for a simply supported beam with a mid-span point load:

$$w = \frac{P \cdot L^3}{48 \cdot E \cdot I} \qquad \text{……..…… (3.1)}$$

where P is the mid-span load, L is the length of the beam between supports, and I is the area moment of inertia of the cross-section. Solving for the modulus of elasticity yields:

$$E = \frac{P \cdot L^3}{48 \cdot w \cdot I} \qquad \text{……..…… (3.2)}$$

The key results were an average modulus E_x of 4.108×10^5 psi and an average modulus of rupture R of 6300 psi.

3.1.2 Internal Bond Tests

Modified internal bond tests (i.e. tension perpendicular to the face surface) were run to determine the internal bond strength and the out of plane modulus E_y of the hardboard as per ASTM D1037. Ten specimens were randomly cut out of the sample materials provided by the manufacturer to into 2 in. × 2 in. square pieces. The test specimens were glued between aluminum blocks and the assembly was then pulled in tension. To measure the deformation of each sample, standard internal bond test blocks (2 in. × 2 in.) were machined to allow an MTS 632.13B-20 extensometer to be mounted to the side of the blocks. The extensometer was then securely attached to the blocks to prevent it from slipping during the test. Load and deflection from the extensometer were recorded by a computer data acquisition system for each test until specimen failure. A sketch of the aluminum test blocks and hardboard assembly is shown in Figure 7.

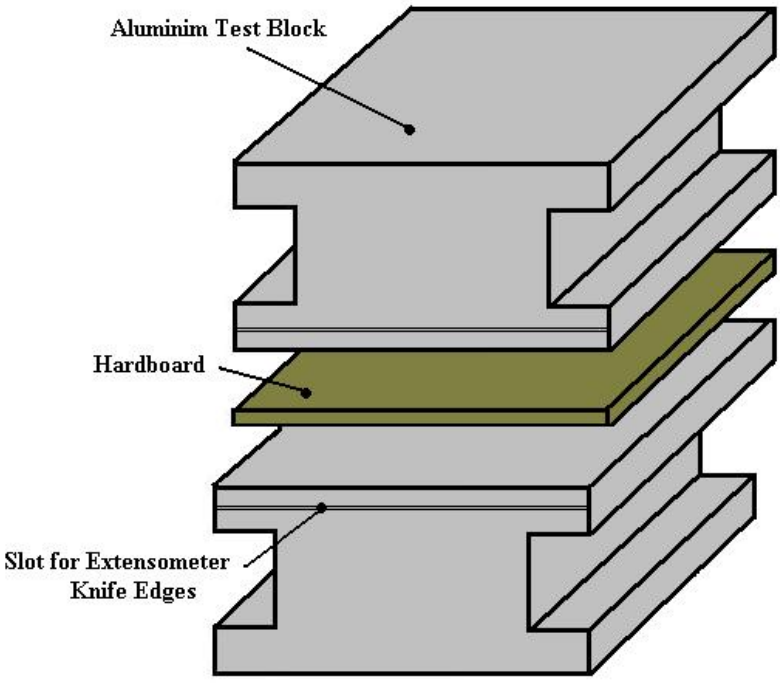

Figure 7: Sketch of Tests Blocks and Hardboard Assembly.

The actual test setup is shown in Figure 8 below. A typical load versus deflection curve for the internal bond tests is shown in Figure 9.

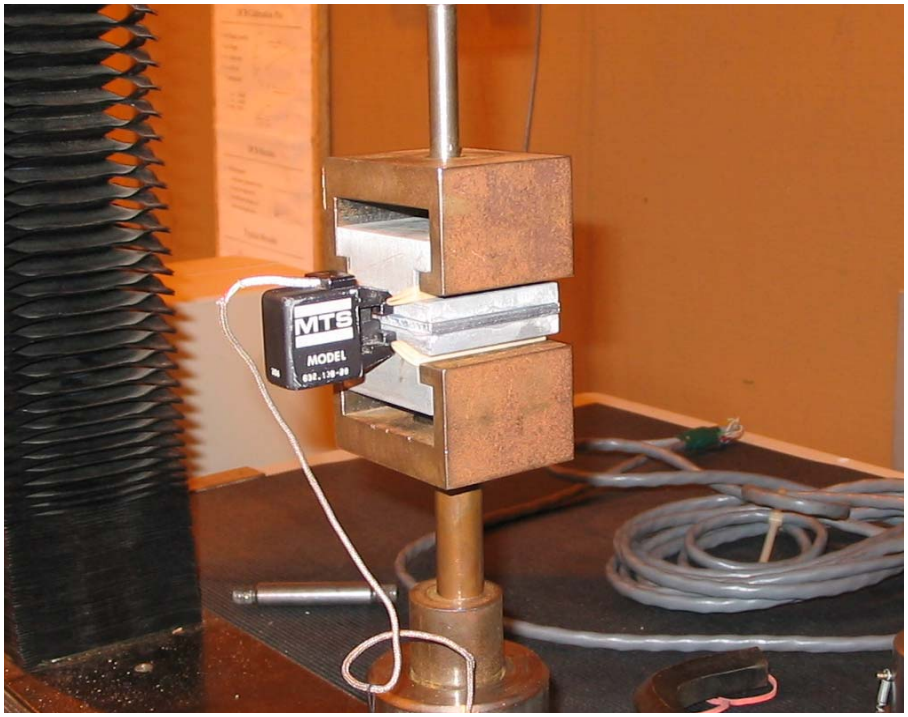

Figure 8: Internal Bond Test

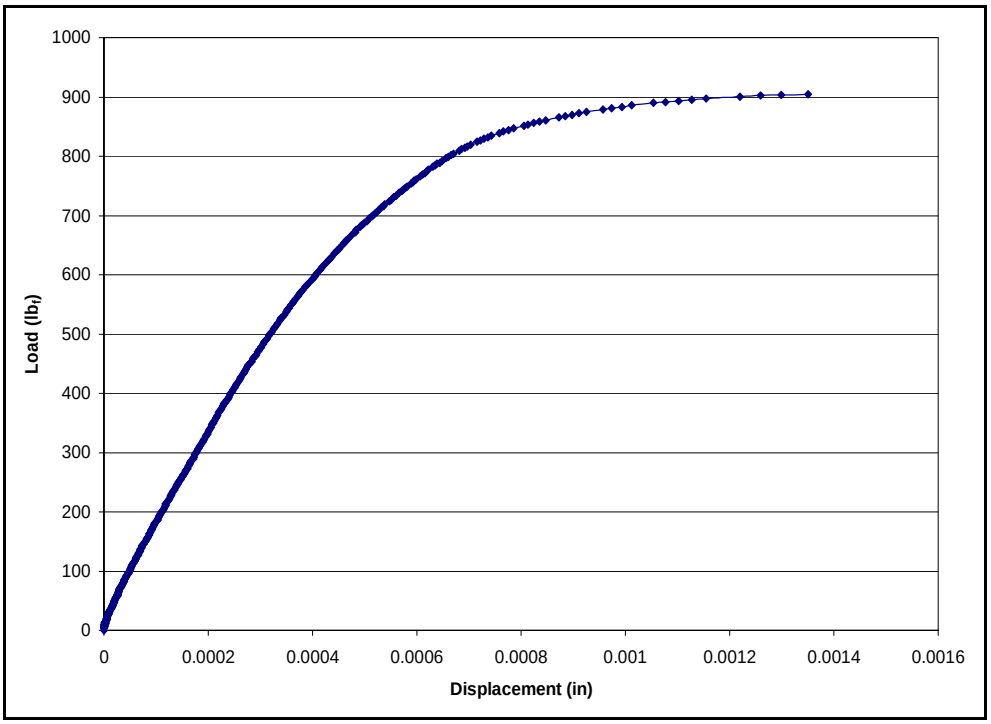

Figure 9: Load Versus Displacement for Internal Bond Tests

The linear region of the load versus deflection curve was used to determine the out of plane modulus E_y, and the maximum load reached was used to determine the internal bond strength. The modulus E_y was computed assuming the axial load was evenly distributed across the test specimen cross-sectional area. For simple axial tension, the elongation of the member is given by:

$$\delta = \frac{P \cdot L}{A \cdot E} \qquad \text{……...…} \quad (3.3)$$

where P is the tensile load, L is the axial length of the test specimen, and A is the cross-sectional area. Solving for the modulus of elasticity yields:

$$E = \frac{P \cdot L}{\delta \cdot A} \qquad \text{……...…} \quad (3.4)$$

The key results were an average modulus E_y of 4.682×10^4 psi and an average internal bond strength of 217 psi. The coefficients of variation for the modulus E_y and internal bond strength were 19.5% and 13.3% respectively.

Assumptions for the tests were that all the deformation occurs in the hardboard panel and that a uniaxial stress state was present. However, in plane stresses σ_x and σ_z will most likely occur, as the hardboard cannot freely contract in the x or z directions as the faces are glued to the test blocks.

The scatter in the data was due to the geometry restrictions (flat plates) for the test samples; however no other method to test for the out of plane modulus was feasible. The panel is produced by pressing wood fibers at an elevated temperature, so a “bar” of the material cannot be made.

3.1.3 Poisson's Ratio Testing

To determine the Poisson's ratios for the hardboard, tension tests were done on rectangular specimens, measuring load, longitudinal strain, and transverse strain. The Poisson's ratios are defined as the relationship between the passive and active strains where active strain is in the loading direction and passive strain is in the non-loaded transverse direction. The Poisson ratio is calculated as:

$$\nu_{ij} = -\frac{\varepsilon_j}{\varepsilon_i}$$

where ε_i is the strain in the loading direction and ε_j is the strain in the unloaded direction of interest ($i,j = x,y,z$ with $i \neq j$). To measure the value ν_{xz}, ten rectangular specimens were cut to dimensions of 1 in. × 10 in. An Instron 4468 universal testing machine was used to pull the specimens in tension (Figure 11). An MTS 632.11B-20 extensometer was used to measure the longitudinal strain and an MTS 632.13B-20 extensometer was used to measure the transverse strain. A typical plot of lateral versus longitudinal strain is shown in Figure 10. The key result was an average Poisson's ratio $\nu_{xz} = 0.121$.

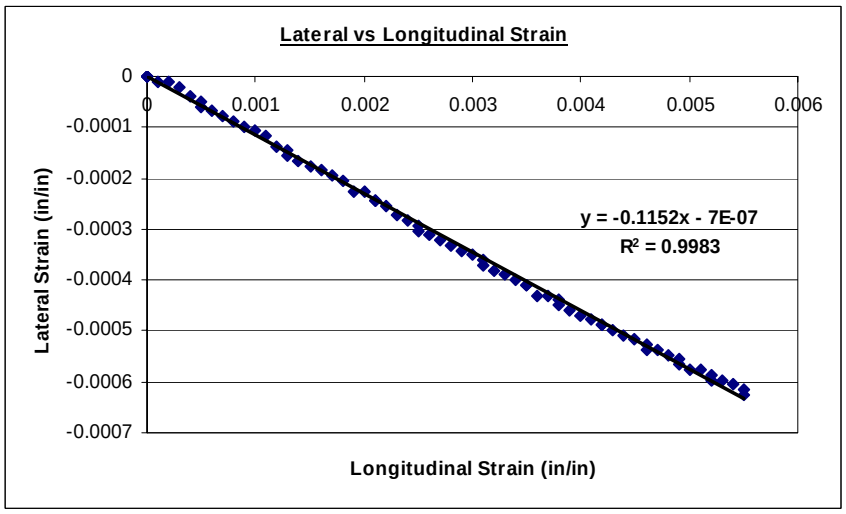

Figure 10: Poisson's Ratio ν_{xz} Test

Figure 11: Test Setup for Measurement of ν_{xz}

To measure the value ν_{xy}, ten rectangular specimens were cut to dimensions of 0.25 in. × 5 in. A United SFM-100kN universal testing machine was used to pull the specimens in tension (Figure 12). A United EB.1-.05 extensometer was used to measure both the longitudinal and transverse strain. The key result was an average Poisson's ratio $\nu_{xy} = 0.0867$.

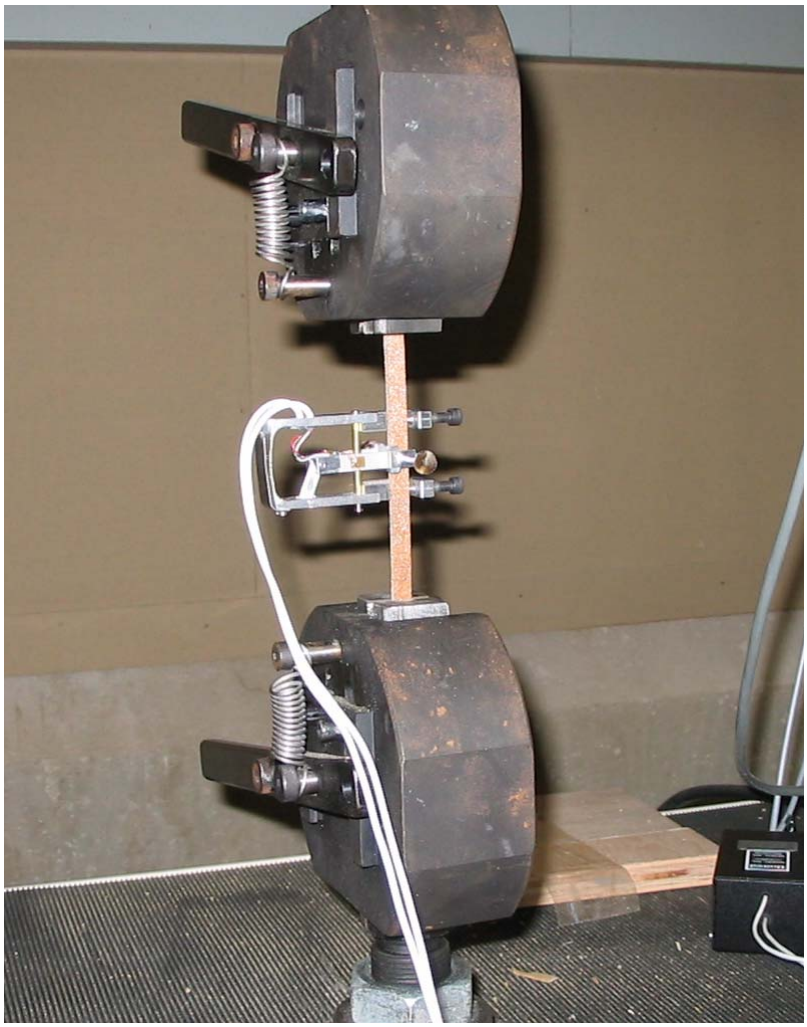

Figure 12: Test Setup for Measurement of ν_{xy}

This test provided some unexpected and yet interesting results. Figure 13 below shows the results of one of the tests for ν_{xy}. As the longitudinal strain increased, the specimen contracted, stopped, and then began to expand. In this case, the specimen expanded beyond its original thickness. To check and make sure that this phenomenon was not a result of equipment malfunction, a piece of aluminum was tested. The aluminum sample showed linear elastic behavior until yield as expected. One theory proposed as to why the hardboard behaves in this manner is that the when material is heated and then pressed in manufacture, the fibers are packed together and residual compressive stresses are present. When failure in tension begins to occur, these stresses are released and the material expands.

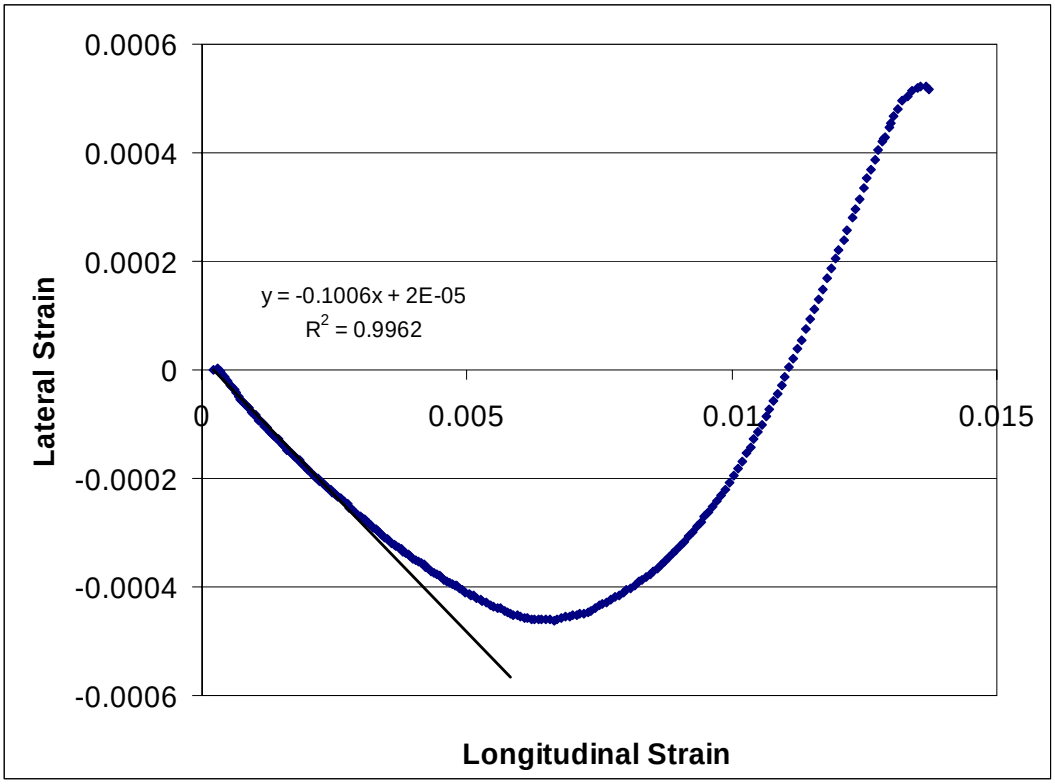

Figure 13: Poisson's Ratio ν_{xy} Test

3.1.4 Hardboard Material Property Testing Summary

The values needed to construct a transversely isotropic model of the hardboard are summarized in Table 2. The modulus of rupture, tensile strength, and internal bond strengths were also measured, and are R = 6305 psi, σ_{ut} = 3680 psi, and σ_{IB} = 215 psi. Referring back to the ANSI A135.4 standard in Table 1, these strengths classify the hardboard as Class 1 Tempered: the highest quality. This shows that the material used in the manufacturing of the door was not of poor quality, but the opposite. It is of the highest quality currently being produced.

Table 2: Hardboard Material Properties

Material Property	Mean Value	Std. Dev.	Coef. Var. %
E_x (psi)	4.108×10^5	6644	1.6
E_y (psi)	4.682×10^4	9105	19.4
E_z (psi)	4.108×10^5	6644	1.6
G_{xy} (psi)	3.268×10^4	-	-
G_{yz} (psi)	3.268×10^4	-	-
G_{xz} (psi)	1.832×10^4	-	-
ν_{xy}	0.087	0.023	26.2
ν_{yz}	0.010	-	-
ν_{xz}	0.121	0.014	11.6

3.2 Glue / Stile Stiffness

Bending tests were performed to help predict the failure of the hardboard when loaded in bending and glued to a stile. The data from these tests was used to calibrate the theoretical model developed to determine the affect of stile width on stresses in the hardboard door skin.

A 5 in. span was used for all bending tests. The hardboard was tested first as a simply supported beam on the wood stiles, but not glued. These specimens were loaded only elastically to provide a baseline for computing the elastic stiffness of the glue line. Then the hardboard specimens were glued to a set of stiles and tested in bending until failure. The stiles were clamped down to prevent movement during the test. Figure 14 below shows the test setup.

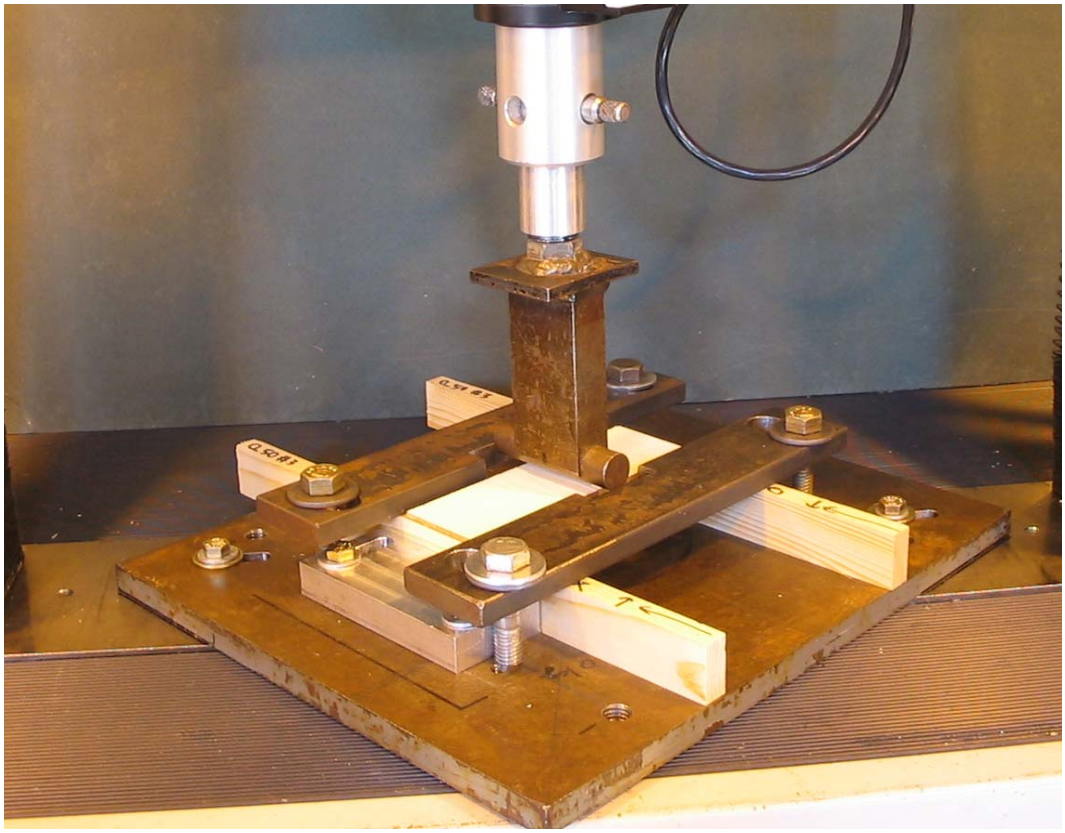

Figure 14: Glued Bend Test Setup

To accomplish this testing, fifteen specimens were randomly cut out of the sample materials provided by the manufacturer. A series of stiles were created; all were $1^1/_8$ in. deep and five each were ½, ¾, and $1^1/_8$ in. wide. These widths were selected as representative final trimmed thicknesses found in sample doors.

Load versus deflection curves for a specimen supported on ½ in. stiles are shown in Figures 15 and 16. From the test data, the slope of the load versus deflection curves for both the unglued and glued cases were calculated. Using these slopes, the bending stiffnesses for both the unglued and glued support conditions were found. A summary of the average results is given in Table 3 below.

Table 3: Glue / No Glue Bend Test Results

Stile Width (in.)	Statistics	Modulus, E (psi)	Bending Stiffness, S: No Glue, S_{NG} (lbf/in.)	Bending Stiffness, S: Glued, S_G (lbf/in.)	Stiffness Ratio S_G / S_{NG}
	Mean	4.369×10^5	74.54	240.31	3.60
$1\ ^1/_8$	Std. Dev.	*80837*	*12.43*	*25.96*	*0.15*
	Coef. Var. %	*18.4*	*16.7*	*10.8*	*4.0*
	Mean	4.092×10^5	68.49	220.37	3.30
$^3/_4$	Std. Dev.	*57002*	*12.23*	*41.12*	*0.30*
	Coef. Var. %	*13.9*	*17.9*	*18.7*	*9.0*
	Mean	4.007×10^5	65.39	191.47	2.81
$^1/_2$	Std. Dev.	*71490.62*	*14.02*	*42.51*	*0.54*
	Coef. Var. %	*17.8*	*21.4*	*22.2*	*19.3*

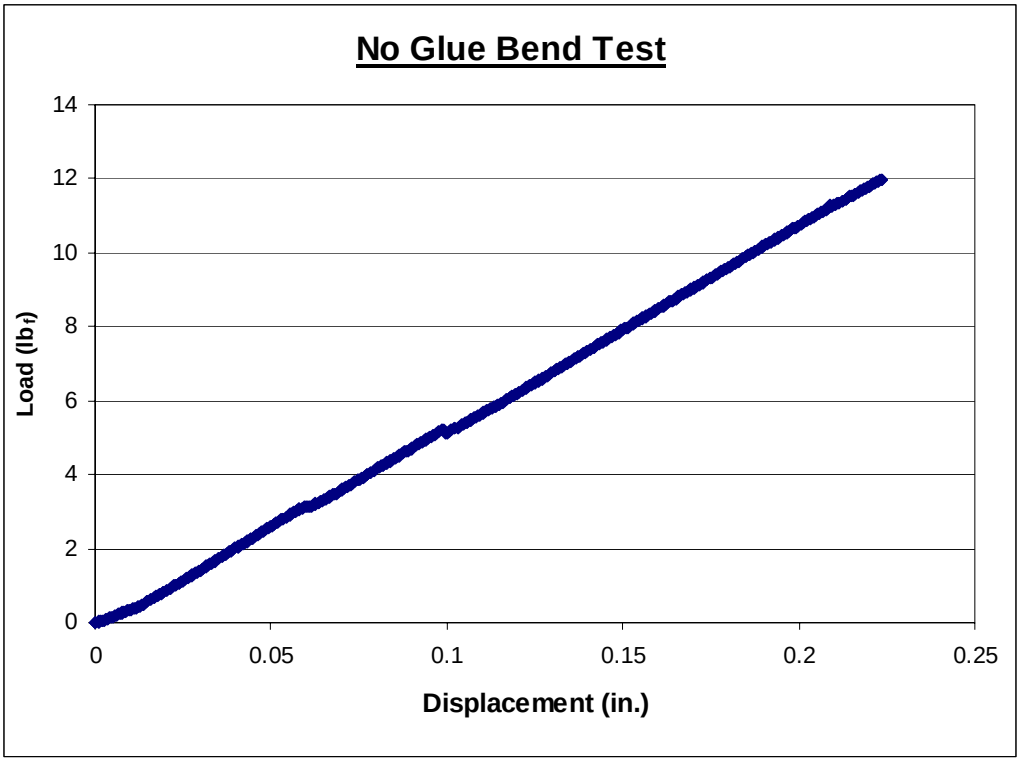

Figure 15: Load Versus Deflection (No Glue)

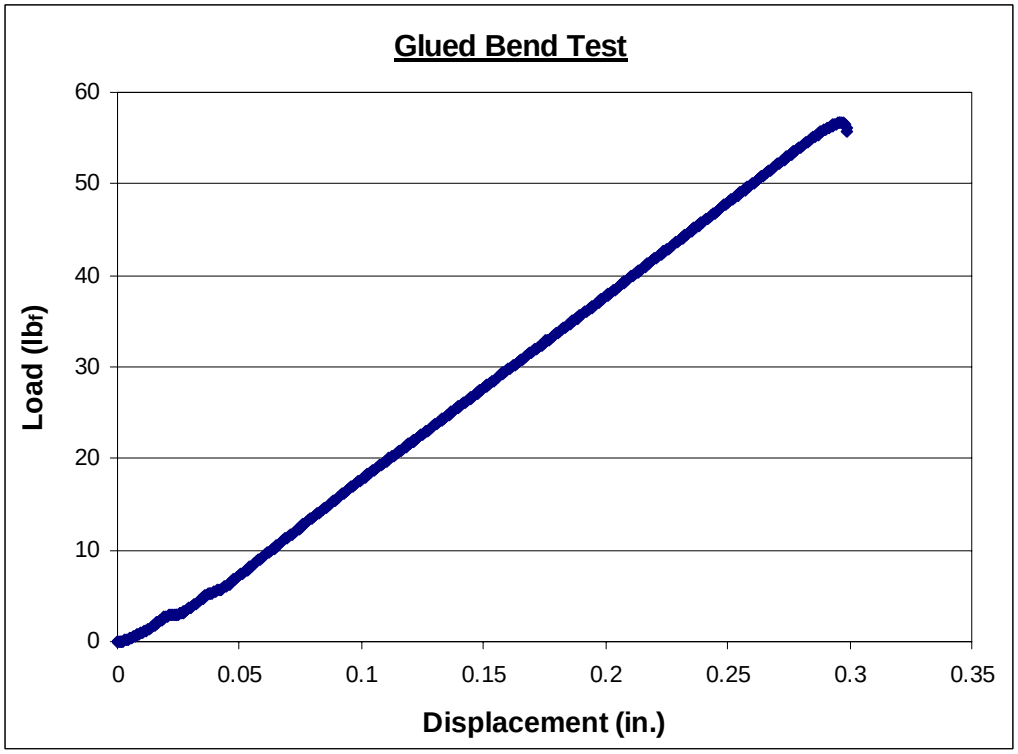

Figure 16: Load Versus Deflection (Glued)

It was expected that the glued specimens would perform somewhere in between the simply supported case and a fixed-fixed support case. This in-between case was modeled as a beam supported by springs at its ends. Knowing the support stiffness for the glued specimens enabled a minimum stile thickness to be calculated to avoid failure.

A key result to note from these tests was that for the ½ in. specimens that were glued to stiles, 4 out of the 5 failed by the splitting of the hardboard just as seen in the actual door products where the stiles were trimmed down below ¾ in. These and only these failed in this manner, and all the other test specimens glued to the wider stiles failed in the middle of the span, as expected for a beam in bending. Failed specimens for ½ in. and ¾ in. stiles are shown in Figures 17 and 18 respectively.

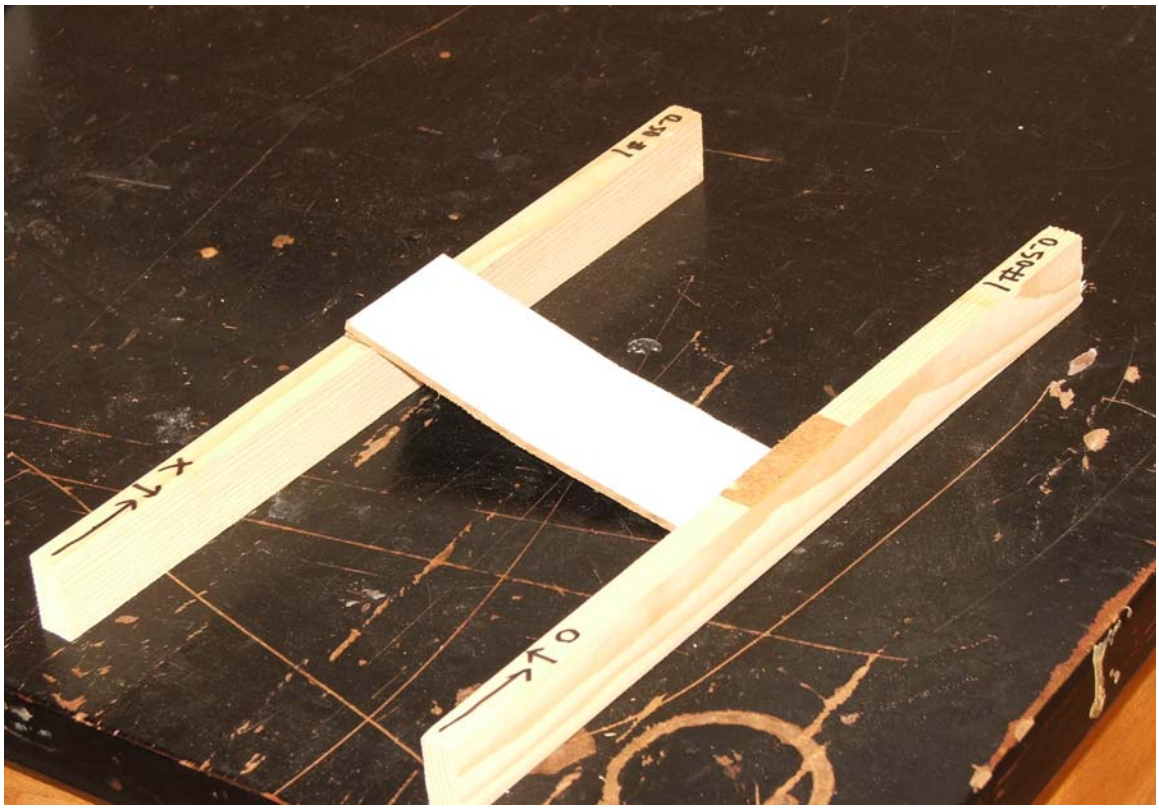

Figure 17: Failed Glued Bending Test Specimen with Stile Width of 1/2 in.

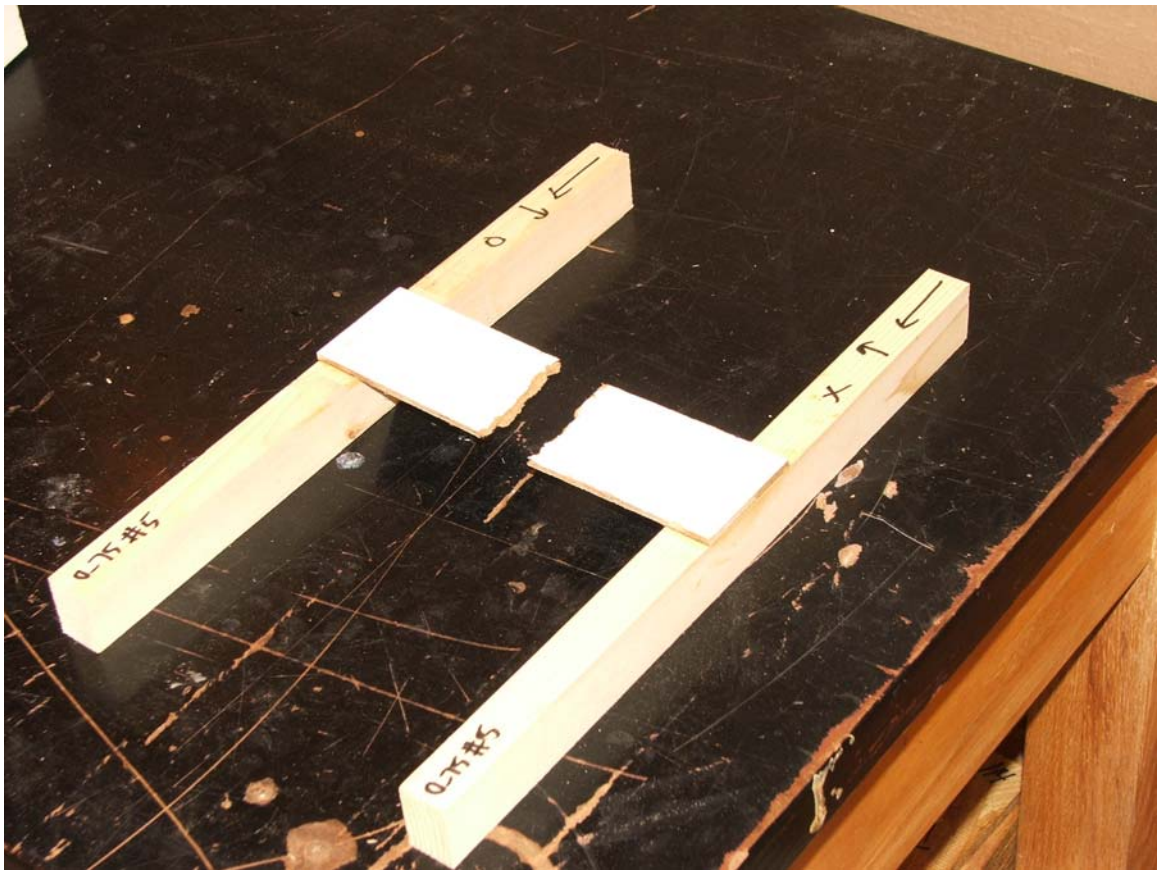

Figure 18: Failed Glued Bending Test Specimen with Stile Width of 3/4 in.

Chapter 4: Finite Element Analysis

4.1 Finite Element Modeling

To predict the stresses developed in the hardboard and stiles due to forces applied in the manufacturing process; a finite element analysis was done using a commercial software package, ANSYS version 8.0. The geometry and loadings of the model were based on the free-body diagram shown in Figure 19 below.

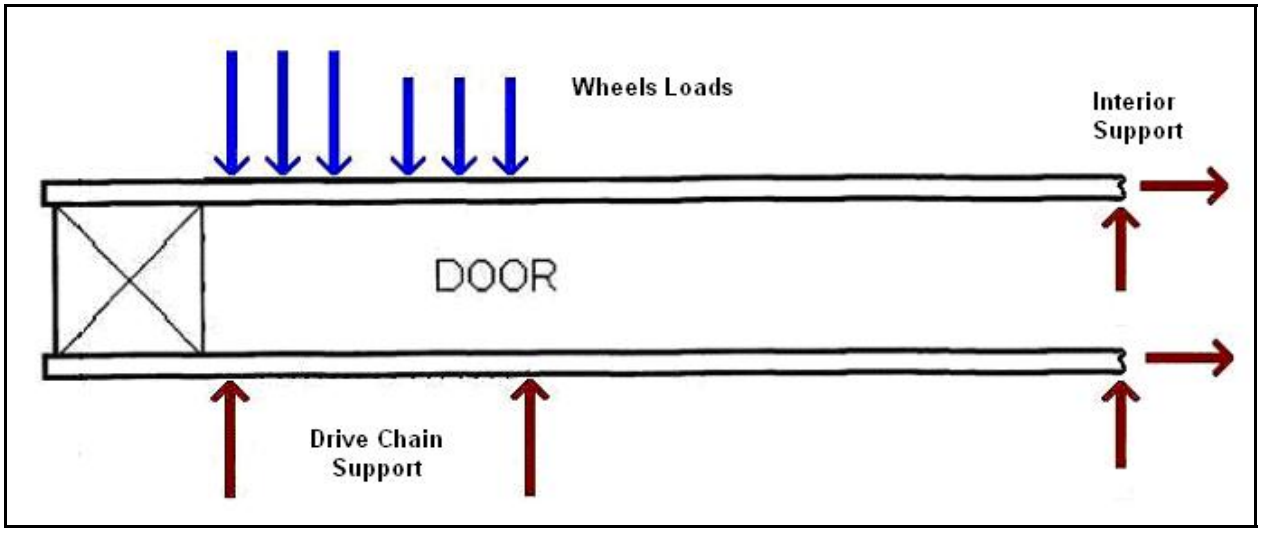

Figure 19: Free Body Diagram of Analyzed Door Section.

4.1.1 Finite Element Method

The finite element method can be used to model a geometrically complex domain of a particular problem as a collection of geometrically simple subdomains, called finite elements. The collection of these elements is called the finite element mesh. Over each finite element, the physical process is approximated by functions and algebraic equations relating physical quantities (such as displacements) at selected points of the elements, called nodes. An approximation for the solution of the governing differential equation, $u(x)$, over the entire domain, x, of the problem is sought as:

$$u \approx U_N \equiv \sum_{j=1}^{N} c_j \phi_j(x) + \phi_O(x) \qquad \text{..... (4.1)}$$

where c_j are coefficients to be determined and $\phi_j(x)$ and $\phi_O(x)$ are functions pre-selected such that the specified boundary conditions of the problem are satisfied by the approximate solution U_N. To do this, the "weak formulation" of the governing differential equation is developed. "A weak form is a weighted-integral statement of a differential equation in which the differentiation is distributed among the dependent variable and the weight function and includes the natural boundary conditions of the problem" [10].

> "In summary, there are three steps in the development of a weak form. In the first, we put all expressions of the differential equation on one side (so that the other side is equal to zero), then multiply the entire equation by a weight function and integrate over the domain of the problem. The resulting expression is called the weighted-integral form of the equation. In the second step, we use integration by parts to distribute the differentiation evenly between the dependent variable

and the weight function, and use the boundary terms to identify the form of the primary and secondary variables. In the third step, we modify the boundary terms by restricting the weight function to satisfy the homogeneous form the specified essential boundary conditions and replacing the secondary variables by their specified values" [10].

For the problem of finding the stresses in the doors, a plane elasticity model was used. The differential equations for the problem include the equilibrium equations, the strain-displacement relations, and the stress-strain relations. The equilibrium equations are given as:

$$\frac{\partial \sigma_x}{\partial x} + \frac{\partial \sigma_{xy}}{\partial y} + f_x = 0 \qquad \text{……...…… (4.2)}$$

$$\frac{\partial \sigma_{xy}}{\partial x} + \frac{\partial \sigma_y}{\partial y} + f_y = 0 \qquad \text{……..……. (4.3)}$$

where f_x and f_y are the body forces per unit volume along the x and y directions respectively, and σ_x, σ_y, and σ_{xy} are the in-plane stresses in the body. The strain-displacements relations are:

$$\varepsilon_x = \frac{\partial u}{\partial x} \qquad \text{…….……..…… (4.4)}$$

$$\varepsilon_y = \frac{\partial v}{\partial y} \qquad \text{……... (4.5)}$$

$$2\varepsilon_{xy} = \frac{\partial u}{\partial y} + \frac{\partial v}{\partial x} \qquad \text{……... (4.6)}$$

where u and v are the in-plane displacements.

The stress-strain relations are:

$$\begin{Bmatrix} \sigma_x \\ \sigma_y \\ \sigma_{xy} \end{Bmatrix} = \begin{bmatrix} c_{11} & c_{12} & 0 \\ c_{12} & c_{22} & 0 \\ 0 & 0 & c_{66} \end{bmatrix} \cdot \begin{Bmatrix} \varepsilon_x \\ \varepsilon_y \\ 2\varepsilon_{xy} \end{Bmatrix} \qquad \text{……...…… (4.7)}$$

where c_{ij} are the elasticity (material) constants for an orthotropic material with principal material directions coinciding with the coordinate axes (x, y, z).

The boundary condition are expressed as:

$$\begin{aligned} t_x &\equiv \sigma_x n_x + \sigma_{xy} n_y = \hat{t}_x \\ t_y &\equiv \sigma_{xy} n_x + \sigma_y n_y = \hat{t}_y \end{aligned} \qquad \text{on } \Gamma_2 \qquad \text{……...… (4.8)}$$

$$u = \hat{u} \qquad v = \hat{v} \qquad \text{on } \Gamma_1 \qquad \text{……... (4.9)}$$

where (n_x, n_y) are the direction cosines of the unit normal vector $\vec{n}$ on the boundary Γ_1, $\hat{t}_x$ and $\hat{t}_y$ are specified boundary tractions, and $\hat{u}$ and $\hat{v}$ are specified displacements. Equations (4.2) and (4.3) can be expressed in terms of just the displacements by substituting equations (4.4) through (4.6) into (4.7), and the results into (4.2) and (4.3):

$$\begin{aligned} -\frac{\partial}{\partial x}\left(c_{11}\frac{\partial u}{\partial x} + c_{12}\frac{\partial v}{\partial y} \right) - \frac{\partial}{\partial y}\left[c_{66}\left(\frac{\partial u}{\partial y} + \frac{\partial v}{\partial x} \right) \right] &= f_x \\ -\frac{\partial}{\partial x}\left[c_{66}\left(\frac{\partial u}{\partial y} + \frac{\partial v}{\partial x} \right) \right] - \frac{\partial}{\partial y}\left(c_{12}\frac{\partial u}{\partial x} + c_{22}\frac{\partial v}{\partial y} \right) &= f_y \end{aligned} \qquad \text{…….… (4.10)}$$

Following the three step procedure previously discussed, the weak formulation of equations (4.10) becomes:

$$0 = h_e \iint_{\Omega^e} \left[\frac{\partial w_1}{\partial x}\left(c_{11}\frac{\partial u}{\partial x} + c_{12}\frac{\partial v}{\partial y}\right) + \frac{\partial w_1}{\partial y} c_{66}\left(\frac{\partial u}{\partial y} + \frac{\partial v}{\partial x}\right) - w_1 f_x \right] dxdy$$

$$- h_e \oint_{\Gamma^e} w_1 \left[\left(c_{11}\frac{\partial u}{\partial x} + c_{12}\frac{\partial v}{\partial y}\right) n_x + c_{66}\left(\frac{\partial u}{\partial y} + \frac{\partial v}{\partial x}\right) n_y \right] ds \qquad \ldots\ldots\ldots \text{(4.11)}$$

$$0 = h_e \iint_{\Omega^e} \left[\frac{\partial w_2}{\partial x} c_{66}\left(\frac{\partial u}{\partial y} + \frac{\partial v}{\partial x}\right) + \frac{\partial w_2}{\partial y}\left(c_{12}\frac{\partial u}{\partial x} + c_{22}\frac{\partial v}{\partial y}\right) - w_2 f_y \right] dxdy$$

$$- h_e \oint_{\Gamma^e} w_2 \left[c_{66}\left(\frac{\partial u}{\partial y} + \frac{\partial v}{\partial x}\right) n_x + \left(c_{12}\frac{\partial u}{\partial x} + c_{22}\frac{\partial v}{\partial y}\right) n_y \right] ds \qquad \ldots\ldots\ldots\ldots \text{(4.12)}$$

where h_e is the element thickness, Ω^e and Γ^e are the domain and boundary of the element e respectively.

The displacements u and v are approximated over by Ω^e by:

$$u \approx \sum_{j=1}^{n} u_j^e \Psi_j^e(x,y) \qquad v \approx \sum_{j=1}^{n} v_j^e \Psi_j^e(x,y) \qquad \ldots\ldots\ldots \text{(4.13)}$$

The weight functions w_1 and w_2 are defined as:

$$w_1 = w_2 = \Psi_i^e \qquad i = 1, 2, \ldots, n \qquad \ldots\ldots\ldots\ldots\ldots\ldots\ldots\ldots \text{(4.14)}$$

Using the weak form, equations (4.11) and (4.12), the matrix form of the finite element model is constructed as:

$$\begin{bmatrix} [K^{11}] & [K^{12}] \\ [K^{12}]^T & [K^{22}] \end{bmatrix} \cdot \begin{Bmatrix} \{u\} \\ \{v\} \end{Bmatrix} = \begin{Bmatrix} \{F^1\} \\ \{F^2\} \end{Bmatrix} \qquad \text{..... (4.15)}$$

where

$$K_{ij}^{11} = \iint_{\Omega^e} h_e \left(c_{11} \frac{\partial \Psi_i}{\partial x} \frac{\partial \Psi_j}{\partial x} + c_{66} \frac{\partial \Psi_i}{\partial y} \frac{\partial \Psi_j}{\partial y} \right) dxdy$$

$$K_{ij}^{12} = K_{ij}^{21} = \iint_{\Omega^e} h_e \left(c_{12} \frac{\partial \Psi_i}{\partial x} \frac{\partial \Psi_j}{\partial y} + c_{66} \frac{\partial \Psi_i}{\partial y} \frac{\partial \Psi_j}{\partial x} \right) dxdy$$

$$K_{ij}^{22} = \iint_{\Omega^e} h_e \left(c_{66} \frac{\partial \Psi_i}{\partial x} \frac{\partial \Psi_j}{\partial x} + c_{22} \frac{\partial \Psi_i}{\partial y} \frac{\partial \Psi_j}{\partial y} \right) dxdy$$

$$F_i^1 = \iint_{\Omega^e} \left(h_e \Psi_i f_x \right) dxdy + \oint_{\Gamma^e} \left(h \Psi_i t_x \right) ds$$

$$F_i^2 = \iint_{\Omega^e} \left(h_e \Psi_i f_y \right) dxdy + \oint_{\Gamma^e} \left(h \Psi_i t_y \right) ds$$

Finite element analysis software such as ANSYS assembles and populates these matrices, and then solves for the unknowns.

4.1.2 Modeling of the Problem

In the construction of the computer model, PLANE 82 elements, which are two dimensional 8 node structural solid elements were used. The degrees of freedom were the displacements u_x and u_y in the plane of the model. It terms of modeling the different materials and the adhesive interface, different regions were used with differing material properties. However, a region with adhesive properties could not be added to the model. The hardboard and stile are directly connected in the model and elements from each share nodes along the interface. Conrad et al. [8] reviewed a study on the effects of bondline thickness on Mode I fracture toughness, and bondline thicknesses ranged from 60 to 160 micro-meters. Due to the extremely small thickness of the adhesive layer, an independent region could not be incorporated into the model. Attempting to incorporate a region of this thickness created mesh construction problems. An auto mesh generator was used to greatly simplify and reduce the time required for model construction. An attempt to individually specify node locations was completely infeasible for the geometry of the problem. For a thickness of only one thousandth of an inch, problems such as many mis-shapen elements arose while attempting to transition from elements of this size (0.001 in.) and those needed to mesh the remainder of the bulk geometry (0.1 in.). Attempting to mesh the entire model with elements sizes of only one thousandth of inch results in quickly exceeding the number of permitted nodes for use in the software. Hence, a specific adhesive region was not included in the model. This topic is further discussed in Chapter 7, Suggested Future Research.

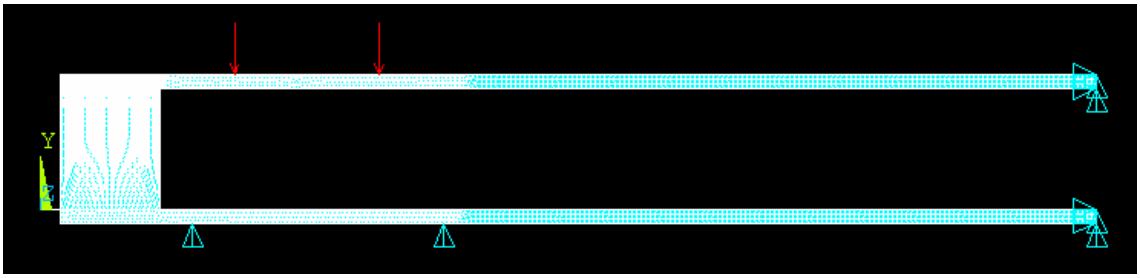

Figure 20: Finite Element Computer Model

Figure 20 above shows the computer model created in ANSYS. An overall model width of 10 in. was used which represents a reasonable spacing to the next interior support of the hardboard face panels. The boundary condition applied at the far right ends was zero displacement in both the *x* and *y* directions. To model the drive chain support used in the sawing process, the vertical displacement of two points on the bottom face panel was set to zero. These represent the left and right edges of the drive chain. This constraint allows the hardboard face panel in between the two support points to deflect upwards, which models the drive chain's inability to pull downward on the bottom panel.

To model the forces applied by the hold down wheels, two forces were applied to the top panel, representing the two wheels pressing down on the panel. These forces were evenly distributed over the width of each wheel. An over force *F* was applied, and was split between the two wheels, with 75% on the left wheel (closest to the stile) and 25% on the right wheel. The uneven distribution was used due to the observed flexibility of the hardboard over the width of the model and the close proximity of the left wheel to the stile. The left wheel will push the panel immediately beneath it downward, and cause the panel immediately below the right wheel to deflect downward also. The right wheel therefore will not load the panel face as heavily as the left wheel. The bottoms of the two

wheels do not move independently of one another. An extreme example would be that if the hardboard were exceedingly flexible, the left wheel would deflect the panel so much that the right wheel would never contact it, and therefore not exert a force on it.

Two sets of material properties were used in the model, one for the hardboard and one for the stiles. The testing for and determination of material properties for the hardboard is discussed in section 3.1. For the stiles, properties for Loblolly Pine were selected from the Wood Handbook [9].

The stiles were modeled as orthotropic materials, and the properties for Loblolly Pine were given in the Wood Handbook [9] for the longitudinal, radial, and tangential material directions. Figure 21 was used to transfer these properties for the stiles into the *x-y-z* coordinate system used in the computer model. For example, the longitudinal modulus, E_L, was input into the computer model as E_z, the shear modulus G_{TR} was input for G_{xy}, etc… The properties of the hardboard were directly acquired in the coordinate system shown in Figure 22.

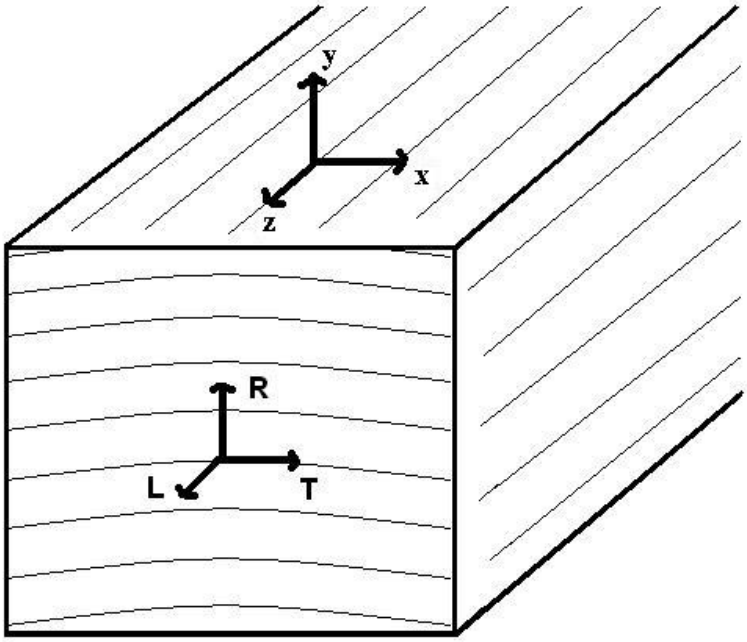

Figure 21: Coordinate System Transfer for the Stiles

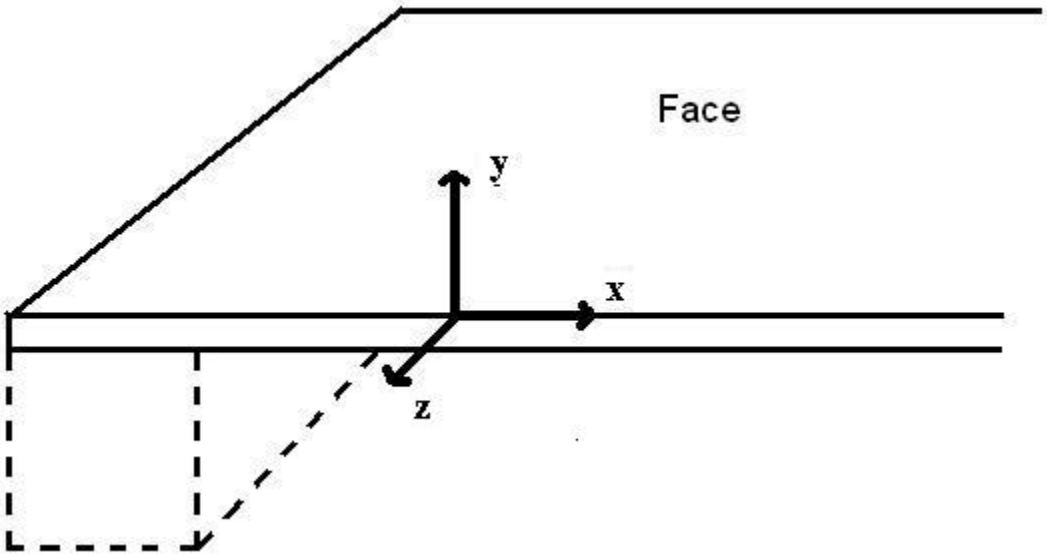

Figure 22: Coordinate System for the Hardboard

4.2 Modeling Limitations

Due to the inability to test for the out-of-plane shear moduli G_{xy} and G_{yz}, limitations must be placed on conclusions drawn from the finite element analysis. The magnitude of the calculated stresses had a non-negligible dependence on the values of the untested shear moduli. The estimation of these from the properties of Loblolly Pine is a reasonable assumption, but not exact. Hence, the exact value of the stresses and the internal bond strength cannot be directly compared to predict failure. For example, if the maximum stress developed in a particular case is 200 psi and the internal bond strength is 217 psi, the conclusion that failure will not occur is questionable. The "flip-side" is also true. A maximum stress of 230 psi cannot necessarily be taken to cause failure. However, the trends shown for varying the width of the stile or increasing the load are valid. The trends will be used to show the effects of trimming the stiles to a width below the "book cut." The overall numerical results do correlate well with the know failures for stile widths below ¾ in., but again cannot be taken as exact.

Another limitation is that the results only relate to the known failure mode of splitting of the hardboard at the hardboard-stile interface. Other failure modes, such as the hold down wheels punching through the panel, were not investigated.

Finally, the true nature of the loading as previously mentioned is not known exactly. Extensive field measurement would have to be done to provide exact results. The assumed loading is reasonable and a very good approximation, however it cannot be assumed to be exact.

4.3 Modeling Results and Discussion

The failure mode of interest was the splitting of the hardboard at the sawn edge of the hardboard-stile interface. This location is shown in Figure 23 by the cross-hatched circle.

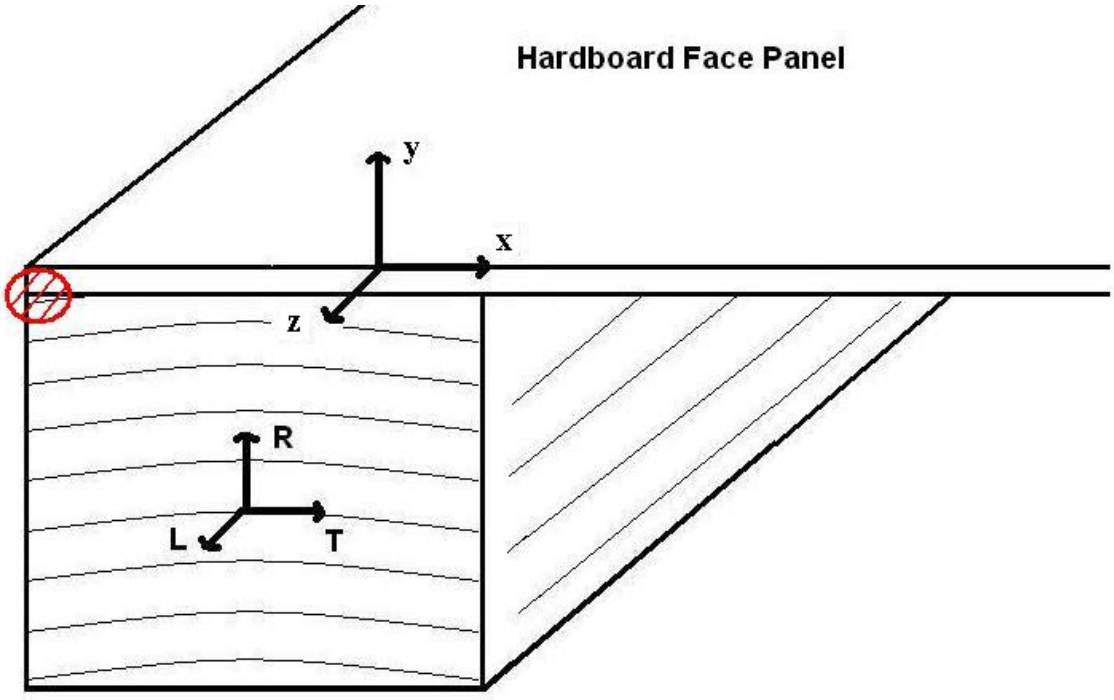

Figure 23: Failure Location of Interest

To determine how stresses develop as the load is applied, multiple force magnitudes and stile widths were "experimented" on by running the model with different geometries. A summary of these is given in Table 4. A stile width of 0.9375 in. corresponds to the "book trim" of $^{3}/_{16}$ in. off of the 1 $^{1}/_{8}$ in. stile width at layup. This will be the maximum stile width expected after sawing.

Table 4: Stile Width, Force, and Maximum Stress (from FEA)

Stile Width (in.)					
$^{1}/_{2}$		$^{3}/_{4}$		$^{15}/_{16}$	
Force (lbf)	Max. Stress (psi)	Force (lbf)	Max. Stress (psi)	Force (lbf)	Max. Stress (psi)
0	0	0	0	0	0
5	82	10	33	15	17
10	164	20	67	30	33
20	317*	30	100	45	50
30	464*	40	133	60	69
40	600*	50	167	80	92
-	-	60	200	-	-
-	-	70	225	-	-
-	-	80	280*	-	-

* Value above the ultimate strength of the hardboard.

Using the data in Table 4, a series of plots were made to show the dependence of the magnitude of the stresses on the forces and stile width. Plots of the stress versus the force applied are shown in Figure 24. A key result shown is that as the stile width decreases, the slope of the stress versus force curve increases. This means that for a given force, as the stile width decreases, the stress in the hardboard increases. If the stress exceeds the internal bond strength of the hardboard, the material will fail by splitting as seen in the sample doors.

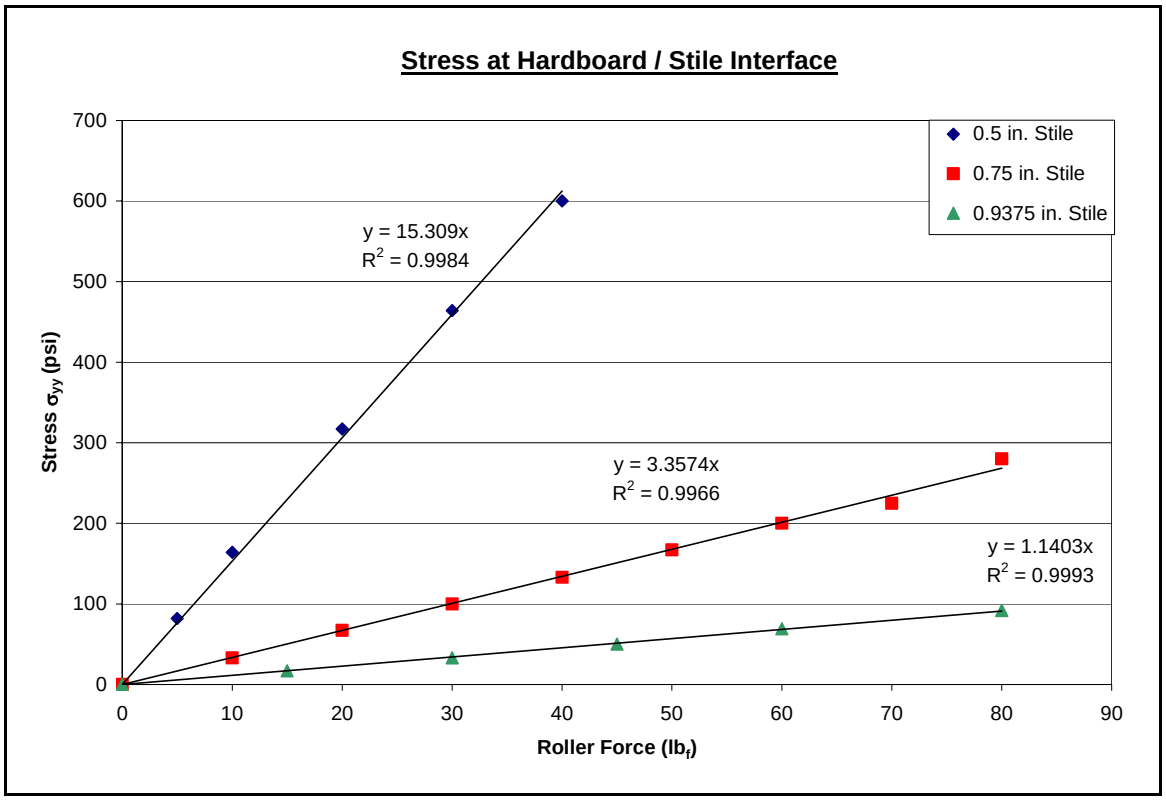

Figure 24: Stress versus Applied Force for Different Stile Widths

This increasing slope was expected, but as seen in Figure 25, the slope appears to increase exponentially, not linearly.

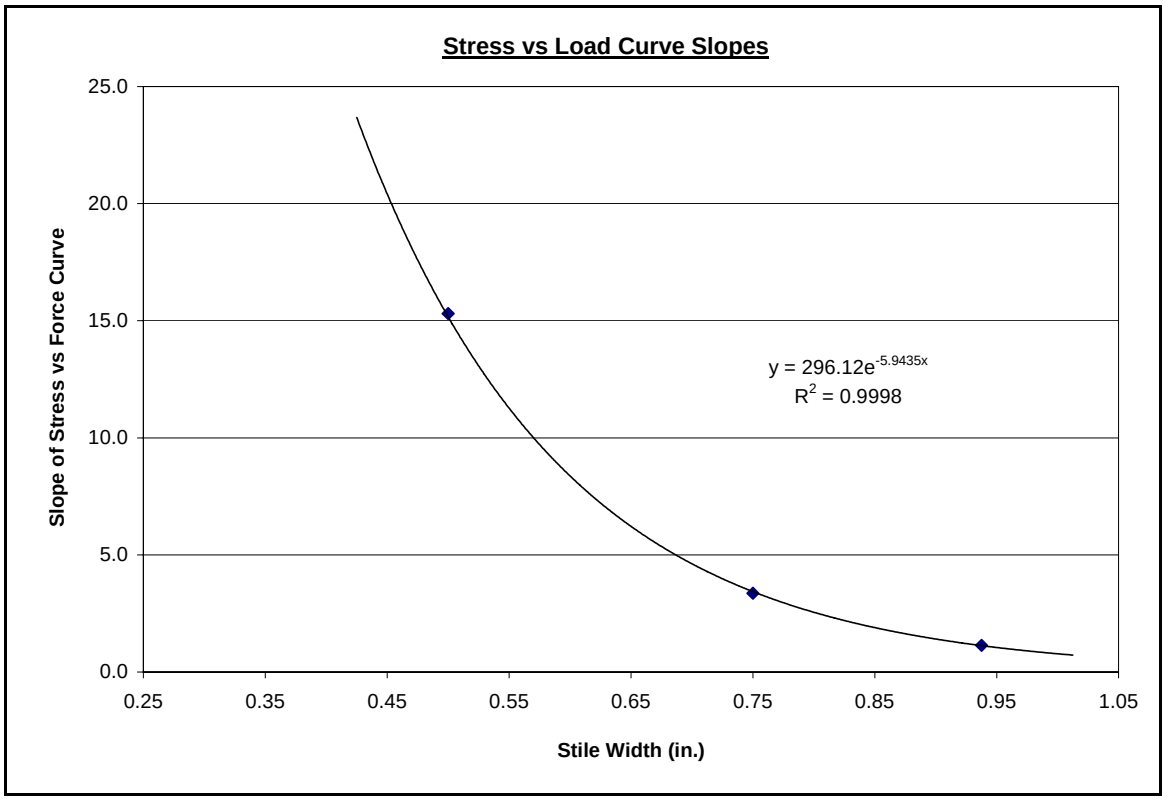

Figure 25: Slopes of Stress versus Load Curves

This non-linear and apparently exponential relationship means that if the stile width is reduced by 20%, the stress will not increase by 20%, but much more. Specifically, at a force of 30 lb_f, a reduction from a stile width of 0.9375 in. to 0.75 in. (a 20% reduction) results in a stress increase from 33 psi to 100 psi; a factor of 3. Reducing further from a stile width of 0.75 in. to 0.50 in. results in a stress increase from 100 psi to 464 psi ; a factor of 4.64. Overall, for a force of 30 lb_f, reducing the stile width from 0.9375 in. to 0.50 in. causes a 1400% increase in the stress. Remember, the absolute magnitude of the stresses could be slightly different in the real hardboard; however the % change will be the same.

Another method of presenting this same concept is to plot the stresses as the stile width is reduced. This was done for four different applied forces and is shown in Figure 26.

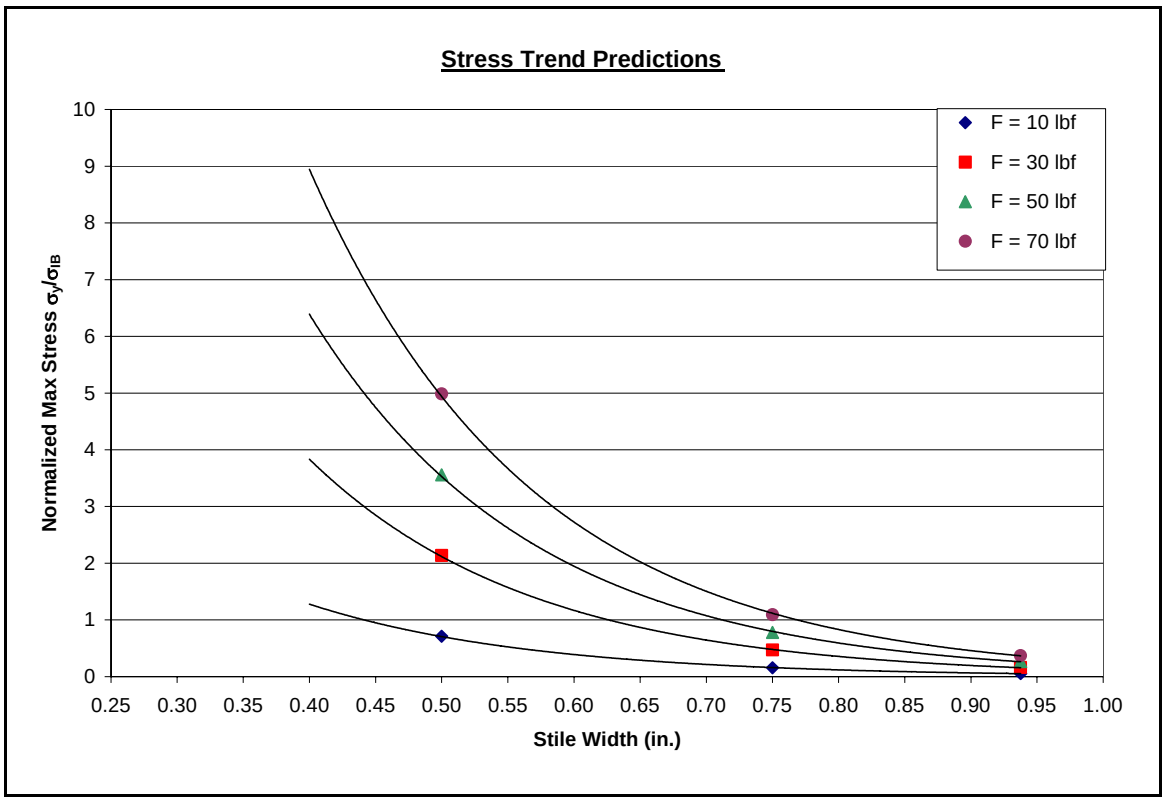

Figure 26: Stress Predictions

The stress values shown have been normalized with respect to the internal bond strength of the hardboard. Any normalized stress value above 1.0 indicates failure. An internal bond strength of 217 psi was assumed, which is the average strength determined from testing. However, this number may be conservative as it was calculated by dividing the load by the cross-sectional area of the test specimen. This assumes a constant stress applied across the entire specimen, which may not be true as perfect alignment of the test setup as well as complete bonding over the entire area of the specimen are not possible. For the 0.9375 in. stile width, increasing the applied force does not dramatically increase

the stress developed in the known failure region. However, as the stile width decreases, increased force leads to much higher stresses. Figure 26 shows that for the "book trim" stile width of 0.9375 in., the failure mode of splitting at the hardboard-stile interface will not occur unless an excessively high force was applied (i.e. greater than 150 lb_f). However, at such high loads, another failure mode will most likely occur first, such as the hold down wheels crushing the hardboard directly beneath them. At a stile width of ¾ in., the edge splitting could occur, depending on the magnitude of the force and the strength of the hardboard. At a stile width of ½ in., splitting of the hardboard will most certainly occur for all but very small forces.

To visualize these results, stress contour plots as shown in Figures 27 and 28 were produced. The different color bands indicate specific stress ranges as shown in the bar at the bottom of each figure. As seen in Figure 27, for a load F of 20 lb_f, the maximum stress reached in the hardboard occurs at the known failure location, and was approximately 317 psi. The horizontal black line indicates the adhesive joint between the stile and hardboard. Hence, the finite element model predicts that the peak stress in the hardboard occurs at the known failure location in the hardboard for a stile width of ½ in. In Figure 28, the load F was 40 lb_f and the peak stress occurs in the interior of the joint, and does not predict failure of the hardboard. The stress distribution pattern, with the peak stress in the interior of the joint as in Figure 28 occurs for all analyses with a stile thickness of ¾ in. and greater. For all analyses done with a stile width of ½ in. such as Figure 27, the peak stress occurred at the known failure location.

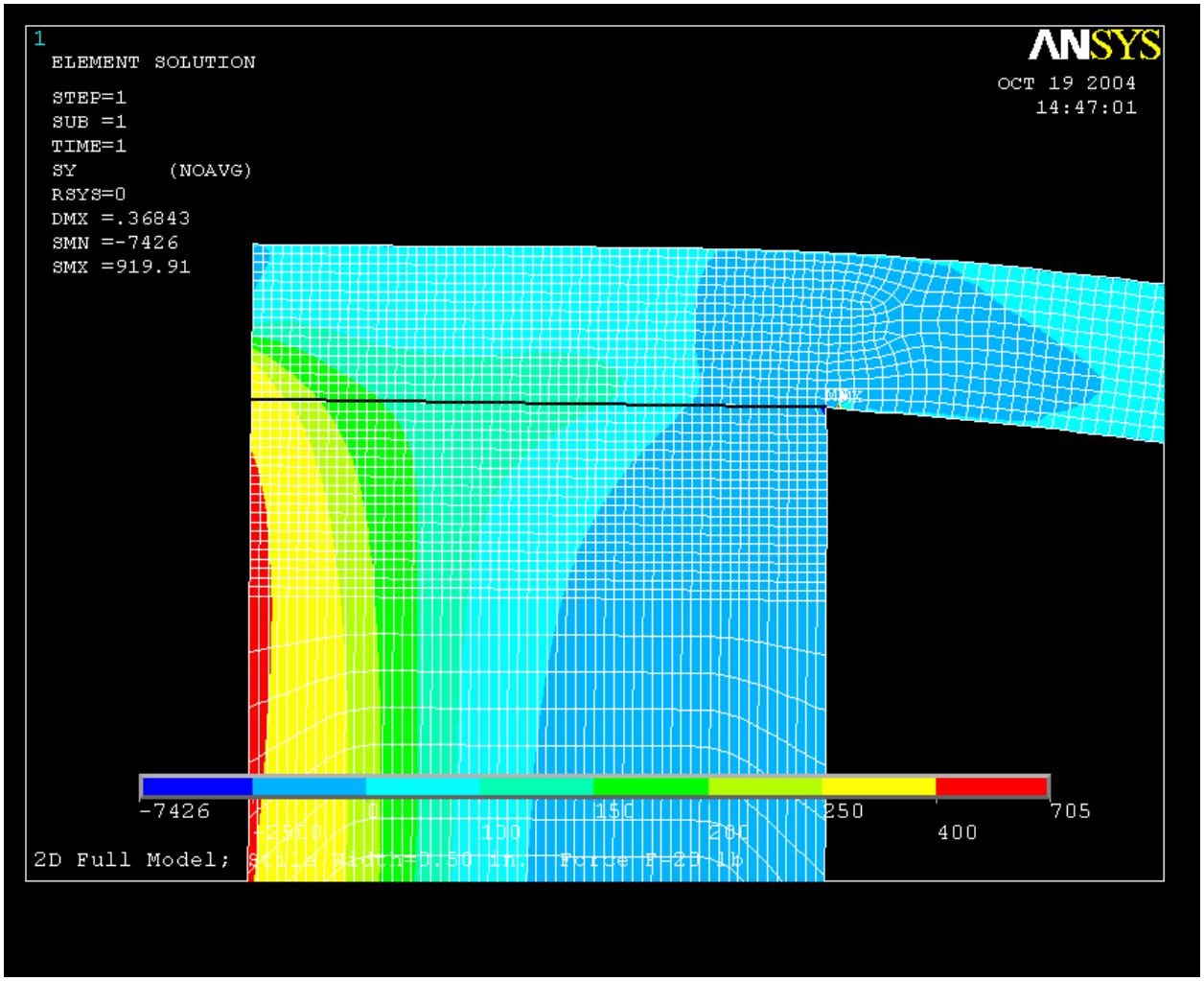

Figure 27: Stress for Stile Width of 0.5 in. and Force F = 20lb$_f$

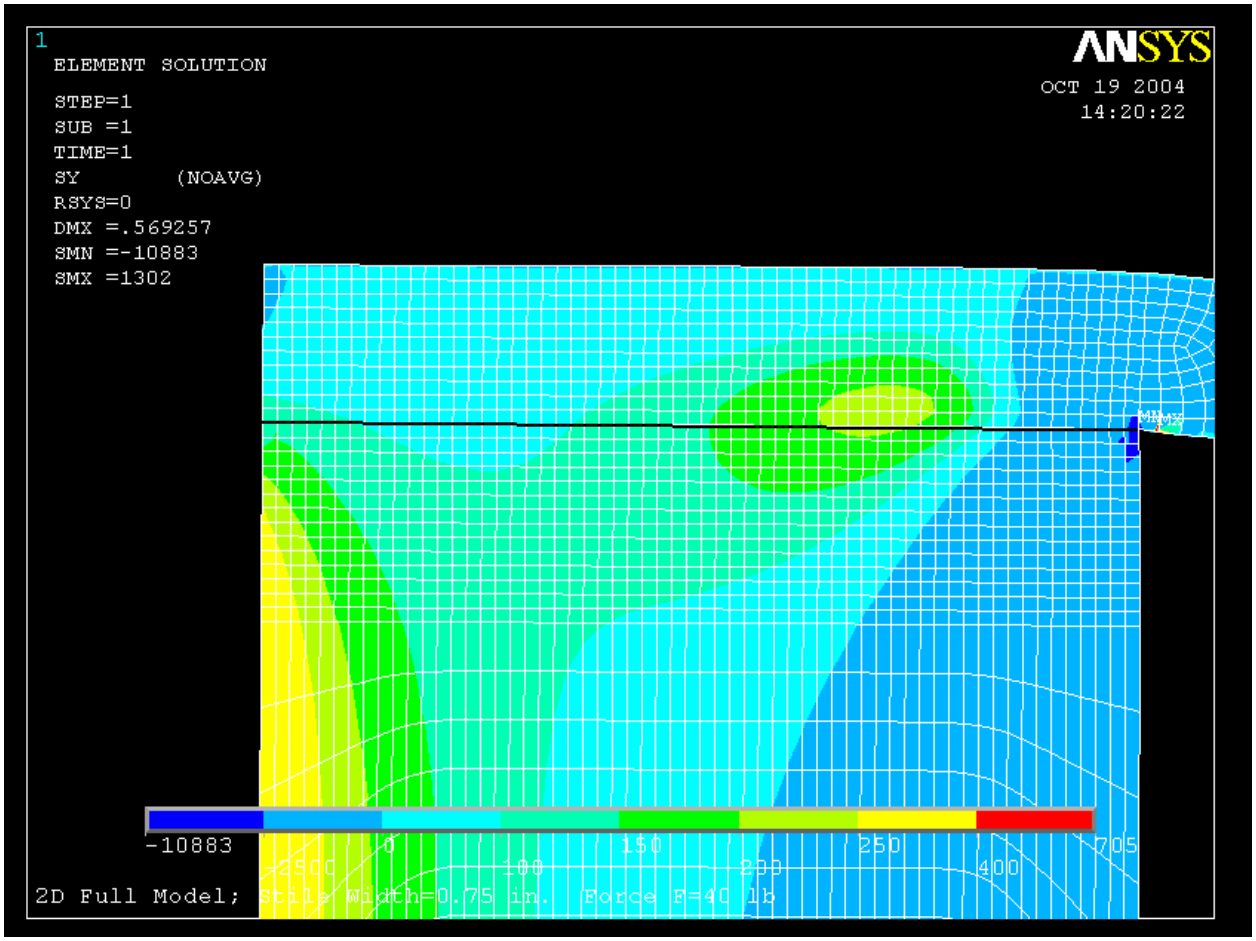

Figure 28: Stress for Stile Width of 0.75 in. and Force F = 40lb$_f$

Chapter 5: Analytical Model

5.1 Model Derivation

The model created to represent the glued joint between the panel and stiles uses the concept of a beam supported on elastic foundations at its ends. Hence, a mechanics of materials approach was used to obtain stresses and deformations. The analysis focused on the determination of a critical stile width that prevents delamination of the hardboard door skin.

Consider a strip of hardboard door skin with both ends uniformly bonded to rigid wooden stiles with an adhesive and subjected to load, P, applied at the mid-span as shown in Figure 29. The width and thickness of the hardboard strip are b and t, respectively, and the width of each adhesive joint is the stile width, a. The span between supports is L, and the total length of the beam is $L+2a$.

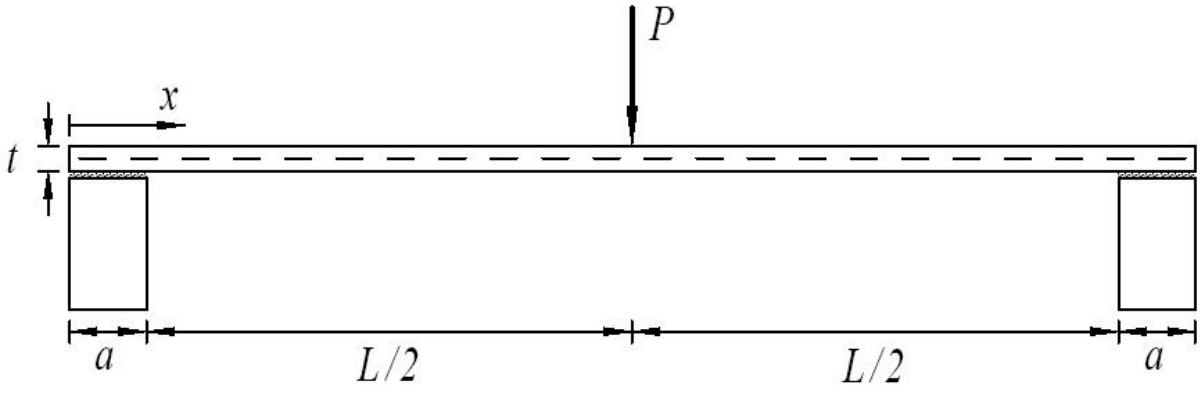

Figure 29: Beam Model of Hardboard Door Skin

The governing differential equations for the vertical displacement functions $w^{(1)}(x)$ in the adhesive joints $(0 < x \le a \quad and \quad L + a \le x \le L + 2a)$ and $w^{(2)}(x)$ in the beam span $(a < x \le L + a)$ are given by (taking into account symmetry in the configuration):

Segment 1: $0 < x \le a$

$$EI\frac{d^4 w^{(1)}}{dx^4} = -k w^{(1)} \qquad \text{……..…. (5.1)}$$

Segment 2: $a \le x < a + \frac{L}{2}$

$$EI\frac{d^4 w^{(2)}}{dx^4} = 0 \qquad \text{…….…….. (5.2)}$$

where EI is the beam flexural rigidity, E is the modulus of elasticity of the hardboard panel, $I = \frac{1}{12}bt^3$ is the area moment of inertia of the cross section, and $k = bk_0$ is the equivalent spring stiffness (force/ unit length/ length) of the adhesive joint (k_0 is expressed in force/ unit length/ unit surface area).

Solutions for the displacement functions are obtained as:

$$w^{(1)}(x) = C_1\cos(\beta x)\cosh(\beta x) + C_2\sin(\beta x)\cosh(\beta x) + C_3\cos(\beta x)\sinh(\beta x) + C_4\sin(\beta x)\sinh(\beta x) \qquad \text{……... (5.3)}$$

$$w^{(2)}(x) = C_5 + C_6 x + C_7 x^2 + C_8 x^3 \qquad \text{……... (5.4)}$$

where $\beta = \sqrt[4]{\frac{k}{4EI}}$ and $C_i \quad i=1,2,3,\ldots 8$ are constants determined by imposing a proper set of boundary conditions.

The expressions for the slope $\theta(x)$, bending moment $M(x)$, and shear $V(x)$ in terms of the displacements function $w(x)$ are obtained as:

$$\theta(x) = \frac{dw}{dx} \qquad \text{..... (5.5)}$$

$$M(x) = -EI\frac{d\theta}{dx} = -EI\frac{d^2w}{dx^2} \qquad \text{..... (5.6)}$$

$$V(x) = \frac{dM}{dx} = -EI\frac{d^3w}{dx^3} \qquad \text{..... (5.7)}$$

The following boundary conditions were applied to solve for the constants C_i:

At $x = 0$, the bending moment and shear force go to zero:

$$M^{(1)} = -EI\frac{d^2w^{(1)}}{dx^2} = 0 \quad \Rightarrow \quad \frac{d^2w^{(1)}}{dx^2} = 0 \qquad \text{..... (5.8)}$$

$$V^{(1)} = -EI\frac{d^3w^{(1)}}{dx^3} = 0 \quad \Rightarrow \quad \frac{d^3w^{(1)}}{dx^3} = 0 \qquad \text{..... (5.9)}$$

At $x = a$, the beam rotates without vertical displacement:

$$w^{(1)} = 0 \quad \textit{and} \quad w^{(2)} = 0 \qquad \text{..... (5.10)}$$

$$\theta^{(1)} = \theta^{(2)} \quad \Rightarrow \quad \frac{dw^{(1)}}{dx} = \frac{dw^{(2)}}{dx} \qquad \text{..... (5.11)}$$

$$M^{(1)} = M^{(2)} \quad \Rightarrow \quad \frac{d^2w^{(1)}}{dx^2} = \frac{d^2w^{(2)}}{dx^2} \qquad \text{..... (5.12)}$$

At x = a+$\frac{L}{2}$, the maximum displacement occurs and the load P is applied:

$$\theta^{(2)} = 0 \quad \Rightarrow \quad \frac{dw^{(2)}}{dx} = 0 \qquad \text{..... (5.13)}$$

$$V^{(2)} = -\frac{P}{2} \quad \Rightarrow \quad \frac{d^3w^{(2)}}{dx^3} = \frac{P}{2EI} \qquad \text{..... (5.14)}$$

Hence, there are 8 boundary conditions needed to solve for the 8 constants C_i.

Applying these 8 boundary conditions results in 8 equations, which are then solved for the 8 unknown constants C_i. The software package Mathematica v5.0 by Wolfram Research, Inc., was used to setup and solve the following equations:

At $x = 0$, the bending moment and shear force go to zero:

$$2C_2\beta^3 - 2C_3\beta^3 = 0 \quad \text{..... (5.15)}$$

$$2C_4\beta^2 = 0 \quad \text{..... (5.16)}$$

At $x = a$, the beam rotates without vertical displacement:

$$C_1\cos(a\beta)\cosh(a\beta) + C_2\cosh(a\beta)\sin(a\beta) + C_3\cos(a\beta)\sinh(a\beta) + C_4\sin(a\beta)\sinh(a\beta) = 0 \quad \text{..... (5.17)}$$

$$C_5 + aC_6 + a^2C_7 + a^3C_8 = 0 \quad \text{..... (5.18)}$$

$$C_2\beta\cos(a\beta)\cosh(a\beta) + C_3\beta\cos(a\beta)\cosh(a\beta) - C_1\beta\cosh(a\beta)\sin(a\beta) + C_4\beta\cosh(a\beta)\sin(a\beta) + C_1\beta\cos(a\beta)\sinh(a\beta) + C_4\beta\cos(a\beta)\sinh(a\beta) + C_2\beta\sin(a\beta)\sinh(a\beta) - C_3\beta\sin(a\beta)\sinh(a\beta) = C_6 + 2aC_7 + 3a^2C_8 \quad \text{..... (5.19)}$$

$$2C_4\beta^2\cos(a\beta)\cosh(a\beta) - 2C_3\beta^2\cosh(a\beta)\sin(a\beta) + 2C_2\beta^2\cos(a\beta)\sinh(a\beta) - 2C_1\beta^2\sin(a\beta)\sinh(a\beta) = 2C_7 + 6aC_8 \quad \text{..... (5.20)}$$

At $x = a + \frac{L}{2}$, the maximum displacement occurs and the load P is applied:

$$C_6 + 2C_7\left(a + \frac{L}{2}\right) + 3C_8\left(a + \frac{L}{2}\right)^2 = 0 \quad \text{..... (5.21)}$$

$$6C_8 = \frac{P}{2EI} \quad \text{..... (5.22)}$$

Solving equations (5.15) through (5.22) leads to the expressions for $w^{(1)}(x)$ and $w^{(2)}(x)$ as follows:

$$w^{(1)}(x) = \frac{L^2 P\left[\cosh(a\beta)\cosh(x\beta)\sin((a-x)\beta) + \cos(a\beta)\cos(x\beta)\sinh((a-x)\beta)\right]}{8EI\beta\left[2+\cos(2a\beta)+\cosh(2a\beta)-L\beta\sin(2a\beta)+L\beta\sinh(2a\beta)\right]}$$

…… (5.23)

$$w^{(2)}(x) =$$

$$\frac{P(a-x)\left\{\left[3L^2-4(a-x)^2\right]\cdot\left[2+\cos(2a\beta)\right]+\left[3L^2-4(a-x)^2\right]\cosh(2a\beta)\right\}}{48EI\left[2+\cos(2a\beta)+\cosh(2a\beta)-L\beta\sin(2a\beta)+L\beta\sin(2a\beta)\right]}$$

$$+\frac{P(a-x)\left\{L(4a+3L-4x)(a-x)\beta\left[\sin(2a\beta)-\sinh(2a\beta)\right]\right\}}{48EI\left[2+\cos(2a\beta)+\cosh(2a\beta)-L\beta\sin(2a\beta)+L\beta\sin(2a\beta)\right]}$$

…… (5.24)

5.2 Equivalent Spring Constant for Adhesive Joints

Due to the additional restraint at the supports provided by the width of the adhesive joints, the overall bending stiffness of the beam increases from that of a simply supported beam, but is bounded by the stiffness of a fully restrained or fixed-fixed beam. The bending stiffness of a beam, from the slope of the linear portion of the load-displacement curve (P-δ) curve is defined as:

$$S = \frac{\Delta P}{\Delta \delta} \qquad \text{..... (5.25)}$$

where ΔP is the change in load and $\Delta \delta$ is the corresponding change in displacement. For a beam of length L subjected to a point load P at the mid-span, the bending stiffness for simply supported beams, S_{ss}, and for fixed-fixed beams S_{ff}, are obtained, respectively, as:

$$S_{ss} = \frac{48EI}{L^3} \qquad and \qquad S_{ff} = \frac{192EI}{L^3} \qquad \text{.... (5.26, a,b)}$$

where EI is the flexural rigidity of the beam cross-section.

The bending stiffness of a beam with both ends supported by adhesive joints (Figure 29) is computed by:

$$S_{kk} = \frac{P}{\delta_{\max}} \qquad \text{..... (5.27)}$$

where $\delta_{\max} = w^{(2)}(a + \frac{L}{2})$ is the maximum displacement at the mid-span (point of application of the load P).

As a result:

$$S_{ss} \le S_{kk} \le S_{ff} \qquad \text{..... (5.28)}$$

which gives the following non-dimensional relation:

$$1 \le \frac{S_{kk}}{S_{ss}} \le 4 \qquad \text{..... (5.29)}$$

The lower limit $\frac{S_{kk}}{S_{ss}} \to 1$ indicates minimum bonding provided by the adhesive layer (k_0 is relatively small) while the upper limit $\frac{S_{kk}}{S_{ss}} \to 4$ indicates perfect and rigid bonding by the adhesive layer (k_0 is relatively large).

Figure 30 shows the variations of the bending stiffness ratio S_{kk} / S_{ss} as a function of the parameter $\rho = k_0 / E$ for various values of width a of the adhesive joints. The parameter ρ (1/length) is used to measure the equivalent spring stiffness k_0 (force/length/unit surface area) of the adhesive layer relative to the elastic modulus E (force/unit area) of the hardboard panel.

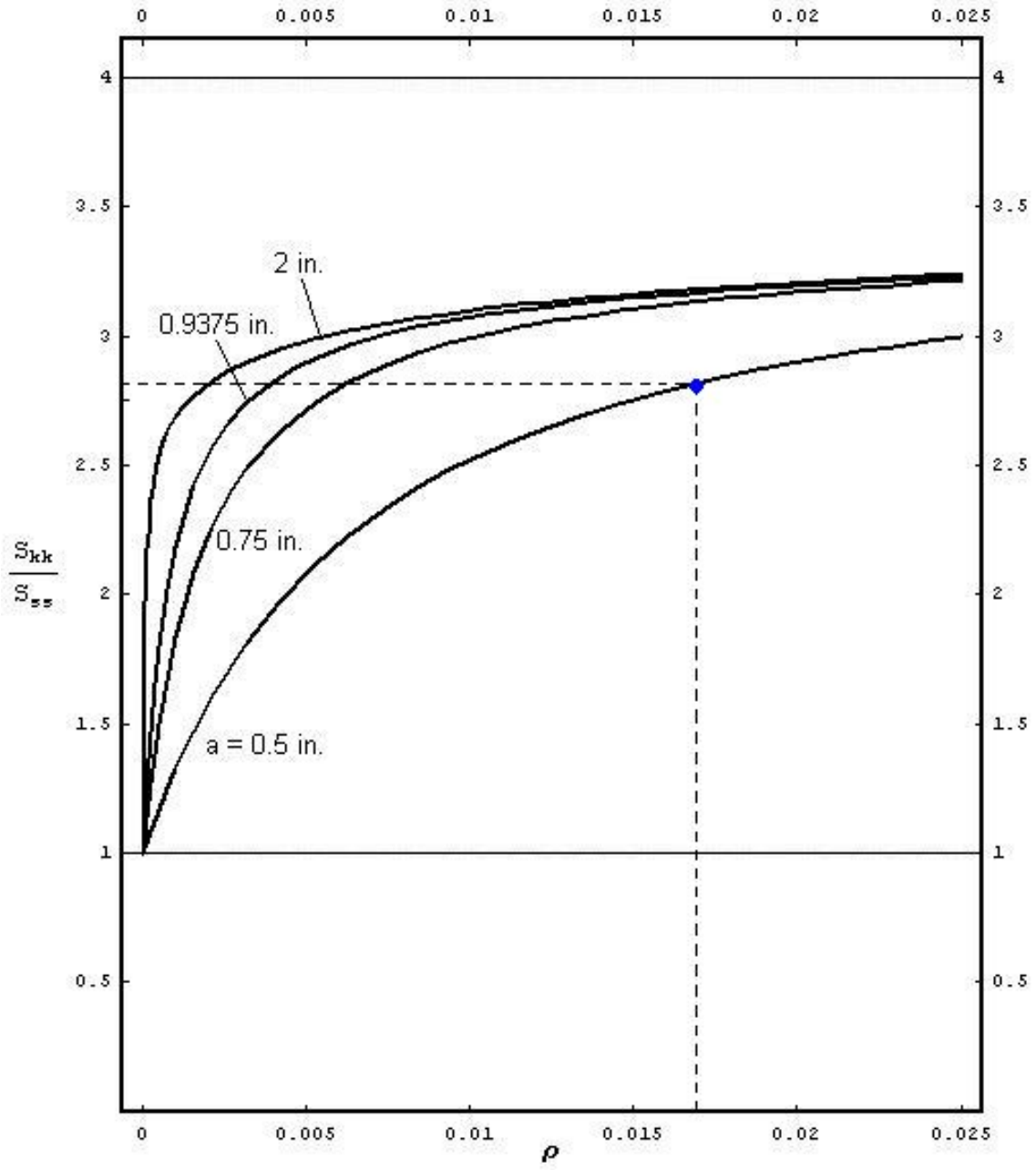

Figure 30: Variations in S_{kk}/S_{ss} as a Function of ρ for Various Widths of the Adhesive Joint

5.3 Modes of Deformation

Depending on the width of the stile, two distinct modes of deformation will occur in the region of the adhesive joint $(0 \le x \le a)$. When the stile is relatively wide, Mode I deformation occurs and the maximum panel displacement occurs inside the region of the adhesive joint $(0 < x \le a)$. Mode II deformation occurs when the width of the stile is relatively narrow and the maximum panel displacement occurs at the outside edge of the stile $(x = 0)$. When subjected to the same loading condition (same *P* and *L*), the maximum displacement under Mode II deformation is much greater than that under Mode I deformation. As a result, Mode I is considered the desirable mode of deformation for the hardboard panel. Figure 31 shows the deformation of the panel for various values of the stile width:

The critical width of the stile a_c that would limit the deformation of the adhesive joint to result in only Mode I deformation and prevent delamination at the outside edge is obtained by finding the stile width a that produces a slope of zero, or $\frac{dw^{(1)}}{dx} = 0$ at the outer edge of the stile $(x = 0)$.

Solving $\frac{dw^{(1)}}{dx} = 0$ at $(x = 0)$ for a yields the following critical stile width a_c:

$$a_c = \frac{\pi}{2\beta}$$

$$a_c = \frac{\pi}{2}\sqrt[4]{\frac{Et^3}{3k_0}}$$

where *t* is the panel thickness, *E* is the modulus of elasticity of the beam, and k_0 is the equivalent spring stiffness (force/unit length/unit surface area) of the adhesive joint.

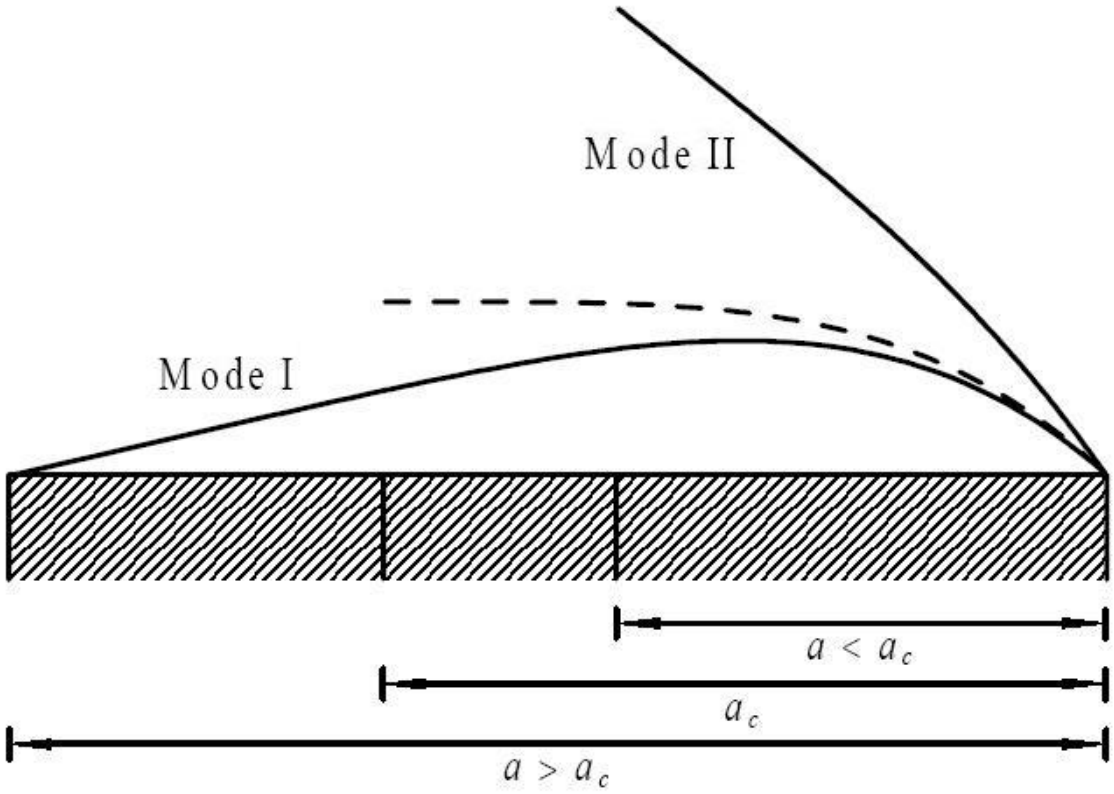

Figure 31: Deformation of the Adhesive Joint for Various Values of Stile Width

$a = a_c$ (critical stile width)

$a > a_c$ (Mode I deformation)

$a < a_c$ (Mode II deformation)

5.4 Closed Form Results

The main objective of the project was to determine the critical stile width needed to ensure the integrity of the door during the manufacturing process. The usual failure mode of the door subjected to manufacturing forces (hold down wheels) was delamination of the hardboard panel at the outer edge of the stile. In general, the delamination could occur under both Mode I and Mode II deformations.

The tensile stress between the panel and the stile is obtained by:

$$\sigma_{yy}(x) = k_0 \cdot w^{(1)}(x)$$

where k_0 is the equivalent spring stiffness and $w^{(1)}(x)$ is the displacement function of the adhesive layer $(0 \le x \le a)$.

The material parameters E and k_0 needed for the stress and displacement analyses were obtained experimentally. The modulus of elasticity E was obtained in bending tests in section 3.1.1 as $E_x = 0.41\times10^6$ psi. The results of the bending tests in section 3.2 yield a stiffness ratio of $\frac{S_{kk}}{S_{ss}} = 2.81$ as obtained from the glued bend tests for a = 0.5 in. This value for a was selected as testing with this value best approximated the assumed boundary conditions. From Figure 30, a value of ρ was obtained as 0.0167 (1/in.). The corresponding value of k_0 is given by:

$$k_0 = \rho E = (0.0167)\cdot(0.41\times10^6) = 6.85\times10^3 \text{ psi/in.}$$

The value for k_0 is a function of the properties of the adhesive joint, and would change if a different adhesive was used.

The maximum tensile stress was found to be much greater in Mode II deformation than Mode I deformation. Figure 32 shows the variations of maximum tensile stress in the hardboard panel as a function of the distance *L* from the inner edge of the stile. When the distance *L* is increased the magnitude of the applied bending moment increases.

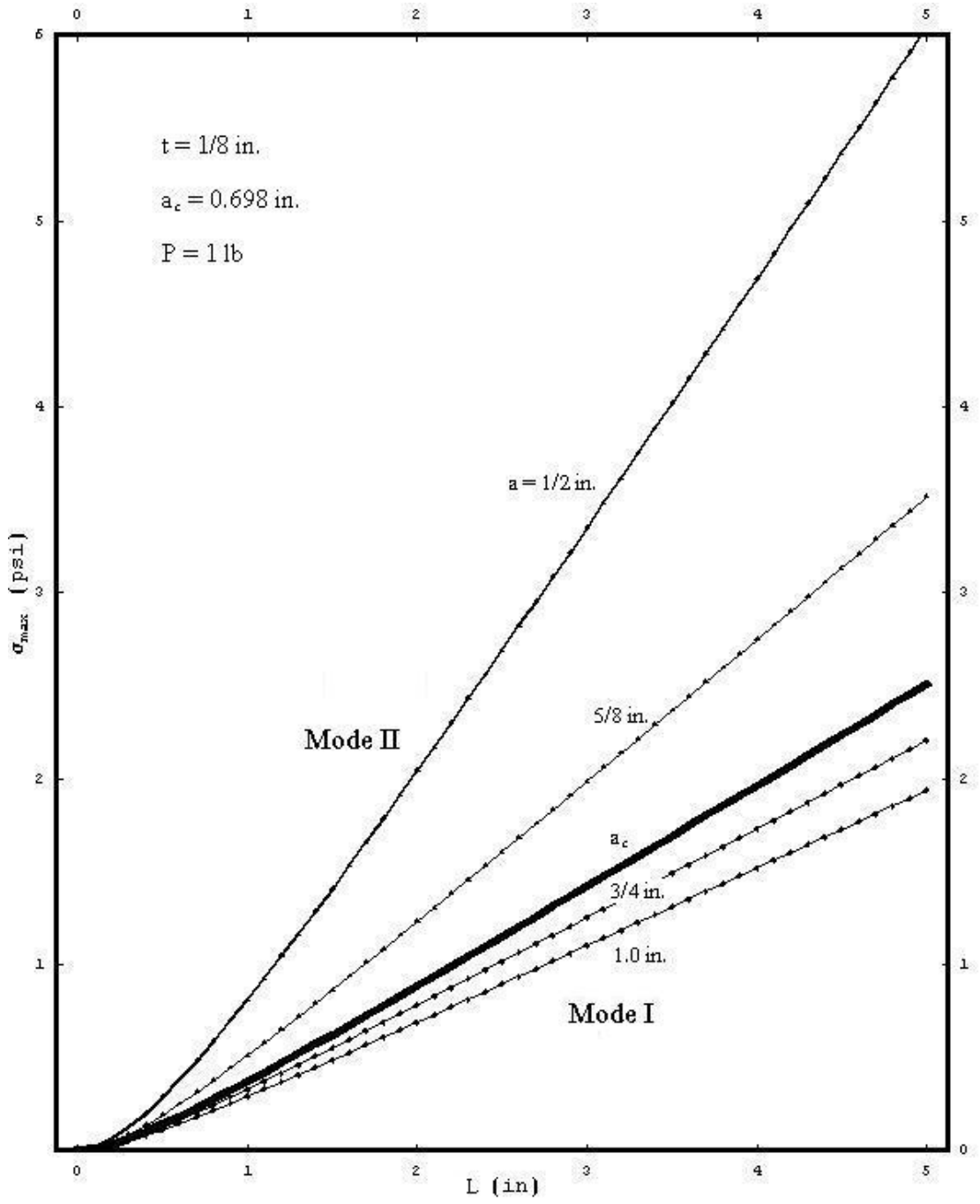

Figure 32: Variations in σ_{max} as a Function of the Distance *D* for Various Stile Widths.

For a decreasing stile width, the magnitude of the maximum tensile stress was found to increase rapidly. Figure 33 plots the variations of the critical stile width a_c as a function of the parameter $\rho = k_0 / E$ for various value of the panel thickness *t*. For a given value of ρ, the critical stile width a_c increases with increasing panel thickness *t*.

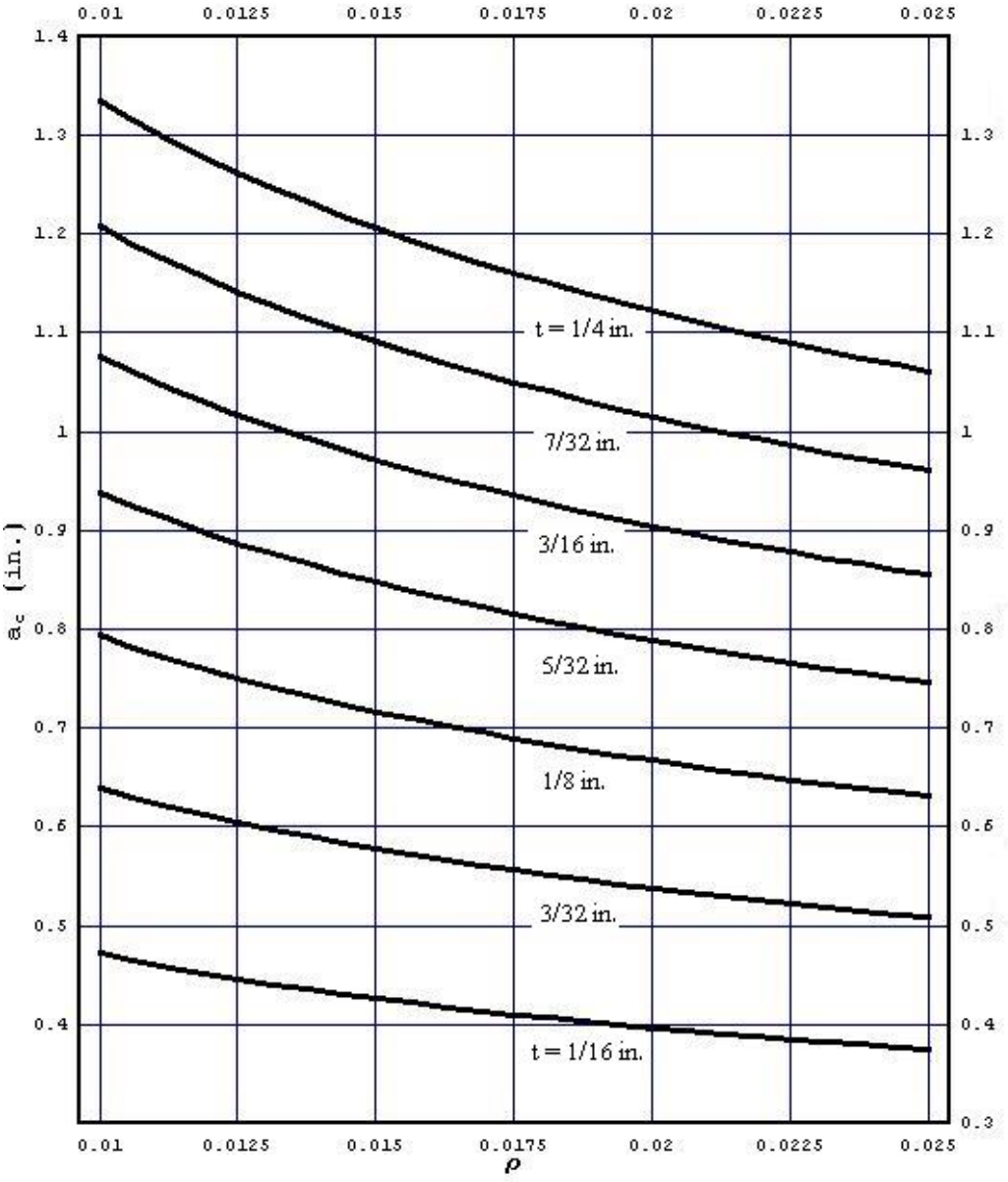

Figure 33: Critical Stile Width a_c as a Function of $\rho = k_0 / E$ for Various Values of Panel Thickness.

Similarly, Figure 34 shows the variations of the critical stile width a_c as a function of the panel thickness *t* for various values of the parameter $\rho = k_0 / E$. For a given value of the panel thickness *t*, decreasing the glue stiffness results in increasing the value a_c, requiring a larger stile width.

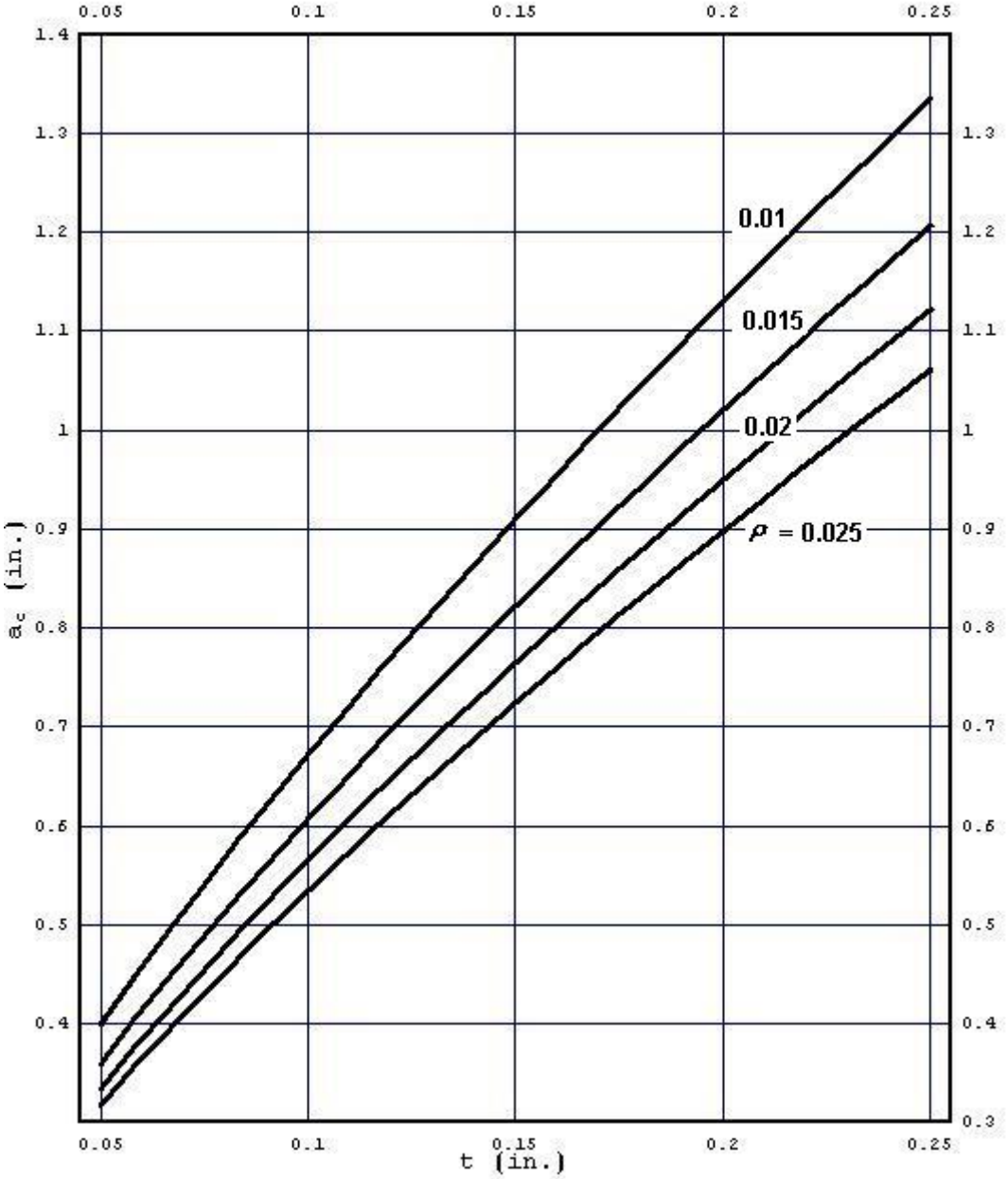

Figure 34: Variation of Critical Stile Width a_c as a Function of Panel Thickness *t* for Various ρ

For the experimentally measured value of $\rho = 0.0167$ (1/in.), Table 5 below gives the critical stile width a_c for various values of the panel thickness *t*.

Table 5: Critical Stile Widths for Various Panel Thicknesses

Panel Thickness, *t* (in.)	$^1/_{16}$	$^3/_{32}$	$^1/_8$	$^5/_{32}$	$^3/_{16}$	$^7/_{32}$	$^1/_4$
Critical Stile Width, a_c (in.)	0.415	0.562	0.698	0.825	0.946	1.062	1.174

Figures 33 and 34 can be used as an effective design tool for selecting the minimum stile width necessary to avoid delamination of the hardboard during the manufacturing process.

Chapter 6: Summary and Conclusions

The objectives of this project were to experimentally determine the engineering properties of the hardboard, develop an engineering model to analyze the stresses and deformations of the door skin/stile assembly, experimentally validate the engineering model, and predict stile widths that will minimize the formation of critical crack producing stresses.

The material properties of the hardboard were measured, and a transversely isotropic model was created based on the results. The shear moduli G_{xy} and G_{yz} were approximated from Lobolly Pine as it was not possible to determine them experimentally. This limits the conclusions that can be drawn from the finite element analysis to observed trends, and prevents direct comparison of calculated stresses to material strengths.

To analyze the stresses and deformation in the hardboard, both a finite element model and a closed form solution based on a mechanics of materials approach were successfully developed. Both analyses provided similar answers regarding the effect of the geometry of the stile and hardboard system on the internal stresses. The closed form solution predicts that as the stile width decreases, the point of maximum deflection, and greatest stresses, moves toward the outside edge of the panel. The critical stile width, or the stile width below which the maximum deflection and stress occurs at the outside edge of the panel, can now be predicted. The finite element model predicts the stresses throughout the entire assembly for a specific loading and geometry, and also shows the outward movement of the maximum stress in the hardboard as the stile width decreases. The closed form solution is more powerful however, as it allows one to design the

hardboard and stile geometry to be able to withstand specific loadings and prevent unwanted delamination of the hardboard during manufacture.

Direct full-scale testing of doors was not done, however the glued bending tests both provided information for the models and verified their results. The observed splitting of the hardboard for only test specimens with ½ in. stile widths, not ¾ in. or wider, supports the prediction of the outward shift of the maximum stress as the stile width decreases. The critical stile width of a_c = 0.7 in. for $^1/_8$ in. hardboard thickness falls between the tested widths of ½ and ¾ in.

The numerical results, such as specific critical stile widths for given hardboard thicknesses, are based on the material properties obtained in the study. However, the model can be applied to any set of materials that behave in a linear elastic manner.

Chapter 7: Suggested Future Research

Four areas for future research on this project include the following: (1) improvement of the test configuration for the glued bending tests to better approximate the assumed boundary conditions, (2) study of the effects of test specimen width on the glued bends tests, (3) research into the non-linear out of plane strain found in conducting tests for Poisson's ratios, (4) measurement of the shear moduli G_{xy} and G_{yz}, and (5) the adhesive joint mesh size transition problem discussed in the finite elements analysis section.

In the glued bending tests, the hardboard beam was assumed to rotate and not deflect at the inner edge of the stile. The stiles were clamped during the test, however possible modification to the test setup could be done to better approximate the assumed boundary conditions. An interior support for the hardboard along the inside face of the stile could be added to strictly enforce the zero deflection desired.

Secondly, the test specimen width that had to be used for the glued bending tests to comply with ASTM D1037 was 2 in. The glued bending test span was only 5 in, and analysis as to the effects of the more plate like geometry as opposed to beam geometry could be researched.

The deformation behavior found in the testing for Poisson's ratio ν_{xy} could be further researched. The apparent expansion of the material under tension is quite an interesting phenomenon and perhaps a better understanding of the behavior of the material from an engineering perspective could be gained from further research into this material response.

Instead of approximating the shear moduli G_{xy} and G_{yz} as discussed in Chapter 3, a test method could be developed to measure the values. This would complete the material model, in that all properties would be measured, and no approximations made for any values. This would also increase the usability of the finite element analysis, as it would remove the restrictions due to the dependence of the calculated stresses on the numerical values of these shear moduli.

Finally, overcoming the problems encountered in creating a specific adhesive layer in the finite element model would be very beneficial and provide a more accurate analysis. A specific adhesive region was not included in the model due to problems with rapid mesh size transition over more than two orders of magnitude from that of the adhesive layer to that of the bulk geometry of the stiles and hardboard. Also, developing a more detailed model such as a three dimensional model could prove to be beneficial in more accurately modeling the problem.

References

1. ASTM, (2003). "ASTM D 1037 Standard Test Methods for Evaluating Properties of Wood-Base Fiber and Particle Panel Materials", American Soc. For Testing and Materials, *Annual Book of Standards, Vol.04.10 Wood*, West Conshohocken, PA.

2. Biblis, E. J. (1989) "Engineering Properties of Commercial Hardboard Siding. Part I. Embossed Panels." *Forest Products Journal*, **39(9)**: 9-13.

3. Boresi, P. A. and Richard J. Schmidt., *Advanced Mechanics of Materials*, 6th ed., John Wiley & Sons, Inc., New York, 2003.

4. Chow, P., Bao, Z., Youngquist, J.A., Rowell, R. M., Muehl, J. A., and Andrzej M. Krzysik., (1996) "Properties of Hardboards Made From Acetylated Aspen and Southern Pine." *Wood and Fiber Science*, **28(2)**: 252-258.

5. Composite Panel Association, (2004), "American National Standard: Basic Hardboard", ANSI Standard A135.4-2004. Gaithersburg, MD. 7p.

6. Composite Panel Association, (2004), "American National Standard: Prefinished Hardboard Paneling", ANSI Standard A135.4-2004. Gaithersburg, MD. 7p.

7. Composite Panel Association, (2005), "Buyer's and Specifiers Guide to North American Particleboard, Medium Density Fiberboard and Hardboard Products and Manufacturers", Gaithersburg, MD. 14p.

8. Conrad, M. P. C., Smith, G. D., and Goran Fernlund. (2004) "Fracture of Wood Composites and Wood-Adhesive Joints: A comparative Review." *Wood and Fiber Science*, **36(1)**: 26-39.

9. USDA, (1999), "Wood Handbook: Wood as an Engineering Material", Gen. Tech. Rep.-GTR-113., US Dep. Of Agriculture, Forest Service, Forest Products Laboratory. Madison WI., 463p.

10. Reddy, J.N., *An Introduction to the Finite Element Method*, 2nd ed., McGraw-Hill, Inc., Boston, Massachusetts. 1993

11. Smardzewski, J. (1999) "Technological Heterogeneity of Adhesive Bonds in Wood Joints." *Wood Science and Technology*, **36**: 213-227.

12. Smith, I., Landis, E. and Meng Gong., *Fracture and Fatigue in Wood*, John Wiley & Sons Ltd., West Sussex PO19 8SQ, England, 2003.

13. Superfesky, M. J. and Wayne C. Lewis.(1974) "Basic Properties of Three Medium-Density Harboards." U.S.D.A. Forest Service Research Paper FPL 238

14. ANSYS Inc., *ANSYS Professional, Academic Version 8.0*. Canonsburg, PA

15. Wolfram Research Inc., *Mathematica, Academic Version 5.0*. Champaign, IL.

Appendix A: Finite Element Analysis Model Code

```
/TITLE,2D Full Model; Stile Width=0.75 in.  Force F=30 lb
/UNITS,BIN
/PREP7

! Model Geometry
*SET,DesiredStileWidth,0.75
*SET,stilewidth,1.125
*SET,stileloss,stilewidth-DesiredStileWidth
*SET,stileheight,1.125
*SET,facethk,0.135
*SET,facelength,10.0
*SET,WheelDist,1.125+0.125
*SET,WheelWidth,7/8
*SET,WheelGap,0.5
*SET,L,stileloss+WheelDist+2*WheelWidth+WheelGap+0.125

!Forces and Distribution
*SET,Force,30
*SET,Fleft,Force*0.75
*SET,Fright,Force*0.25

! KeyPoints
K,1,stileloss,0,0,
K,2,stilewidth,0,0,
K,3,stilewidth,0.85*stileheight,0,
K,4,stileloss,0.85*stileheight,0,
K,5,stilewidth,stileheight,0,
K,6,stileloss,stileheight,0,
K,7,stileloss,stileheight+facethk,0,
K,8,stilewidth,stileheight+facethk
K,10,stileloss+WheelDist,stileheight+facethk,0,
K,11,stileloss+WheelDist+WheelWidth,stileheight+facethk,0
K,12,stileloss+WheelDist+WheelWidth+WheelGap,stileheight+facethk,0
K,13,stileloss+WheelDist+2*WheelWidth+WheelGap,stileheight+facethk,0
K,14,Stileloss+L,stileheight+facethk,0,
K,15,stileloss+L,stileheight,0,
K,16,facelength,stileheight+facethk,0,
K,17,facelength,stileheight,0,
K,18,stileloss,-facethk,0,
K,19,stileloss+WheelDist,-facethk,0,
K,20,L,-facethk,0,
K,21,L+0.125,-facethk,0,
K,22,L+0.125,0,0,
```

```
K,23,facelength,-facethk,0,
K,24,facelength,0,0,

! Areas
A,1,2,3,4
A,3,4,6,5
A,5,6,7,8
A,5,8,10,11,12,13,14,15
A,14,15,17,16
A,1,2,22,21,20,19,18
A,21,22,24,23
APLOT

! Stile Material Properties
ET,1,PLANE82
type,1
*SET,EL,1.8e6
*SET,ET,EL*0.078
*SET,ER,EL*0.113
*SET,GLR,EL*0.082
*SET,GLT,EL*0.081
*SET,GRT,EL*0.013
*SET,vLR,0.328
*SET,vLT,0.292
*SET,vRT,0.382
*SET,vTR,0.362
*SET,vRL,0.037
*SET,vTL,0.0228
MPTEMP,,,,,,,,
MPTEMP,1,0
MPDATA,EX,1,,ET
MPDATA,EY,1,,ER
MPDATA,EZ,1,,EL
MPDATA,PRXY,1,,vTR
MPDATA,PRYZ,1,,vRL
MPDATA,PRXZ,1,,vTL
MPDATA,GXY,1,,GRT
MPDATA,GYZ,1,,GLR
MPDATA,GXZ,1,,GLT

! Face Material Properties
ET,3,PLANE82
type,3
*SET,EX,4.108e5
*SET,EY,46823
*SET,EZ,4.108e5
```

```
*SET,GXY,EX*0.08
*SET,GYZ,GXY
*SET,GXZ,1.832e5
*SET,PRXY,0.0867
*SET,PRYZ,0.0099
*SET,PRXZ,0.121
MPTEMP,,,,,,,,
MPTEMP,1,0
MPDATA,EX,3,,EX
MPDATA,EY,3,,EY
MPDATA,EZ,3,,EZ
MPDATA,PRXY,3,,PRXY
MPDATA,PRYZ,3,,PRYZ
MPDATA,PRXZ,3,,PRXZ
MPDATA,GXY,3,,GXY
MPDATA,GYZ,3,,GYZ
MPDATA,GXZ,3,,EX/(2*(1+PRXZ))

! Meshing
MSHAPE,0
ESIZE,(stilewidth-stileloss)/60
Mat,1
AMESH,2
ESIZE,(stilewidth-stileloss)/60
Mat,3
AMESH,3
ESIZE,(stilewidth-stileloss)/40
Mat,3
AMESH,4
AMESH,6
ESIZE,(stilewidth-stileloss)/10
Mat,1
AMESH,1
ESIZE,facethk/3
Mat,3
AMESH,5
AMESH,7

! Loads and Restraints
SFL,12,PRES,Fleft/WheelWidth,Fleft/WheelWidth,
SFL,14,PRES,Fright/WheelWidth,Fright/WheelWidth,
DK,16,UX,0
DK,16,UY,0
DK,17,UX,0
DK,17,UY,0
DK,19,UY,0
```

```
DK,20,UY,0
DK,23,UX,0
DK,23,UY,0
DK,24,UX,0
DK,24,UY,0


/SOLU
SOLVE
FINISH
/POST1
AVPRIN,0, ,
PLESOL,S,Y,0,1

/CVAL,1,-2500,0,25,50,100,200,250,400
/REPLOT

/CVAL,1,-2500,0,25,50,75,100,200,250
/REPLOT

/REPLOT
/FOC, 1 ,-0.300000,,,1
/REP,FAST
/FOC, 1 ,-0.300000,,,1
/REP,FAST
/FOC, 1 ,-0.300000,,,1
/REP,FAST
/DIST, 1 ,0.729000,1
/REP,FAST
/DIST, 1 ,0.729000,1
/REP,FAST
/DIST, 1 ,0.729000,1
/REP,FAST
/DIST, 1 ,0.729000,1
/REP,FAST
/DIST, 1 ,0.729000,1
/REP,FAST
/FOC, 1 ,,0.300000,,1
/REP,FAST
/DIST, 1 ,0.729000,1
/REP,FAST
/FOC, 1 ,-0.300000,,,1
/REP,FAST
/FOC, 1 ,,0.300000,,1
/REP,FAST
/DIST, 1 ,0.729000,1
```

```
/REP,FAST
!/DIST, 1 ,0.729000,1
!/REP,FAST
```

Appendix B: Hardboard and Stile Material Properties

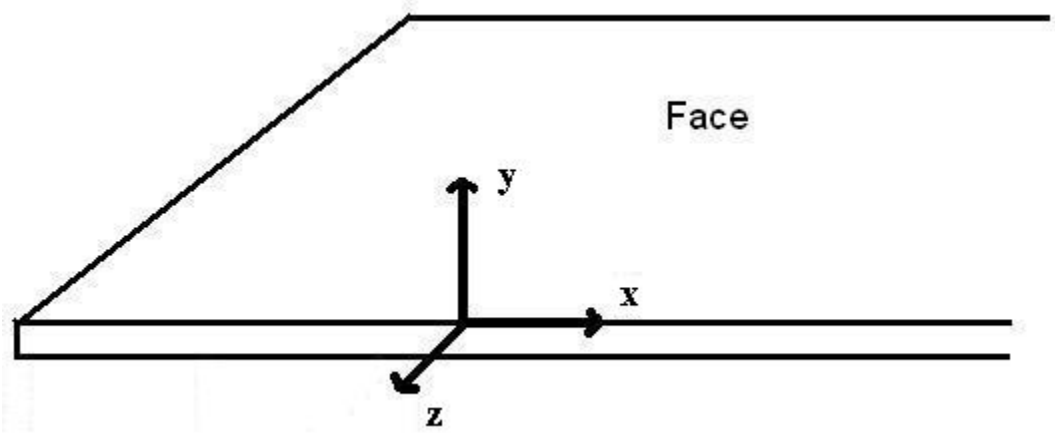

Material Property	Mean Value	Std. Dev.	Coef. Var. %
E_x (psi)	4.108×10^5	6644	1.6
E_y (psi)	4.682×10^4	9105	19.4
E_z (psi)	4.108×10^5	6644	1.6
G_{xy} (psi)	3.268×10^4	-	-
G_{yz} (psi)	3.268×10^4	-	-
G_{xz} (psi)	1.832×10^4	-	-
ν_{xy}	0.087	0.023	26.2
ν_{yz}	0.010	-	-
ν_{xz}	0.121	0.014	11.6

Stile Material Proerties

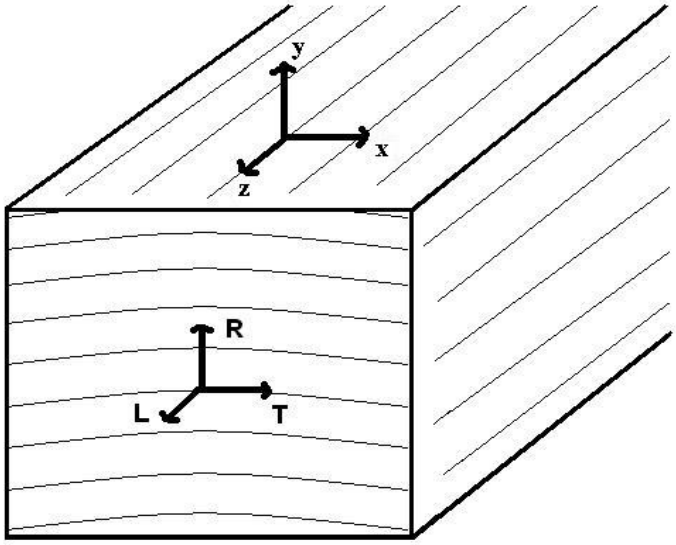

From Wood Handbook (Loblolly Pine):

E_L	1.80E+06	(psi)
E_T	1.40E+05	(psi)
E_R	2.03E+05	(psi)
G_{LR}	1.48E+05	(psi)
G_{LT}	1.46E+05	(psi)
G_{RT}	2.34E+04	(psi)
ν_{LR}	0.328	
ν_{LT}	0.292	
ν_{RT}	0.382	
ν_{TR}	0.362	
ν_{RL}	0.037	
ν_{TL}	0.023	

---------->

E_x	1.40E+05	(psi)
E_y	2.03E+05	(psi)
E_z	1.80E+06	(psi)
G_{xy}	2.34E+04	(psi)
G_{yz}	1.48E+05	(psi)
G_{xz}	1.46E+05	(psi)
ν_{xy}	0.362	
ν_{yz}	0.328	
ν_{xz}	0.023	

Appendix C: Experimental Data

Static Bend Tests

Test	b (in)	d (in)	L (in)	$Mass_i$ (g)	$Mass_o$ (g)	P (lb_f)	P_1 (lb_f)	y_1 (in)	A (in^2)
1	2.0	0.135	3.0	4.41	4.08	55.08	27.11	0.089	9.771
2	2.0	0.135	3.0	4.58	4.22	48.90	25.31	0.086	7.207
3	2.0	0.135	3.0	4.64	4.32	50.01	27.72	0.094	7.431
4	2.0	0.135	3.0	4.59	4.26	53.98	27.30	0.091	9.411
5	2.0	0.135	3.0	4.46	4.15	50.80	25.67	0.086	7.529
6	2.0	0.135	3.0	4.35	4.01	48.73	25.21	0.085	7.516
7	2.0	0.135	3.0	4.44	4.13	48.71	24.92	0.085	6.930
8	2.0	0.135	3.0	4.75	4.41	50.82	27.18	0.089	7.289
9	2.0	0.135	3.0	4.51	4.19	50.38	29.44	0.097	7.472
10	2.0	0.135	3.0	4.75	4.41	53.27	28.94	0.094	8.430

Test	R (psi)	S_{pl} (psi)	E (psi)	W_{ml} (lb_f in/in^3)	% M.C.
1	6799.79	3346.73	417265.19	12.06	8.1
2	6037.26	3124.24	404579.94	8.90	8.5
3	6173.73	3421.68	404204.40	9.17	7.4
4	6664.61	3370.12	409548.03	11.62	7.7
5	6272.08	3169.73	407493.24	9.30	7.5
6	6016.46	3111.90	405310.86	9.28	8.5
7	6013.86	3075.94	403217.33	8.56	7.5
8	6273.82	3356.03	418683.92	9.00	7.7
9	6220.09	3635.05	414999.83	9.22	7.6
10	6577.10	3572.23	422527.82	10.41	7.7
AVG	**6304.88**	**3318.36**	**4.108E+05**	**9.75**	**7.83**
σ	267.28	184.79	6644.19	1.14	0.38
COV	0.04	0.06	0.02	0.12	0.05

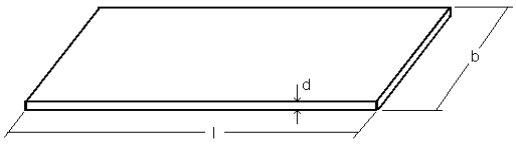

l = 5.0 in

Internal Bond and Modulus Tests

Test #	E (psi)	IntBondStrength
1	37751	170.7
3	57660	258.3
4	61459	197.3
6	37151	192.3
7	45776	226.2
8	41345	225.2
9	51358	217.5
AVG	46823	216.61
STDEV	9115.41	28.80
COV	0.1947	0.1330

In Plane Poisson's Ratio

Test #	Poisson's Ratio (vxz)
3	0.122
4	0.155
5	0.133
6	0.115
7	0.117
8	0.115
9	0.116
10	0.110
11	0.116
12	0.125
13	0.103
AVG	0.121
STDEV	0.014
COV	0.1136

Out of Plane Poisson's Ratio

Test #	Poisson's Ratio (v_{xy})
1	0.101
2	0.062
3	0.060
4	0.049
5	0.094
6	0.101
7	0.112
8	0.068
9	0.121
10	0.079
11	0.103
12	0.091
AVG	0.0867
STDEV	0.0227
COV	0.2613

No Glue Bend Tests

Specimen	Modulus E	Slope of F vs Δ_{mid}
#	(psi)	(lb_f/in)
1_18#1	5.55E+05	87.31
1_18#2	4.86E+05	84.38
1_18#3	3.91E+05	72.30
1_18#4	3.51E+05	55.82
1_18#5	4.15E+05	72.89
0_75#1	4.50E+05	74.49
0_75#2	3.76E+05	70.92
0_75#3	3.54E+05	54.99
0_75#4	3.78E+05	57.59
0_75#5	4.88E+05	84.47
0_50#1	3.30E+05	51.45
0_50#2	3.20E+05	51.97
0_50#3	4.78E+05	84.68
0_50#4	4.50E+05	71.37
0_50#5	4.25E+05	67.47
AVG	4.17E+05	69.47

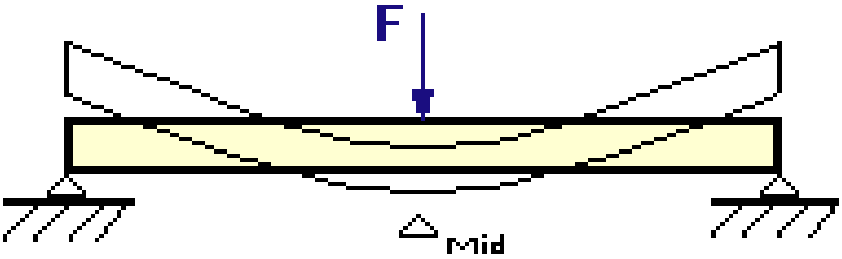

Glued Bend Tests

Specimen	Slope of F vs Δ_{mid}
#	(lb_f/in)
1_18#1	-
1_18#2	-
1_18#3	253.85
1_18#4	210.38
1_18#5	256.70
AVG	*240.31*
0_75#1	-
0_75#2	248.12
0_75#3	198.77
0_75#4	173.62
0_75#5	260.99
AVG	*220.37*
0_50#1	-
0_50#2	172.27
0_50#3	244.77
0_50#4	145.86
0_50#5	202.98
AVG	*191.47*

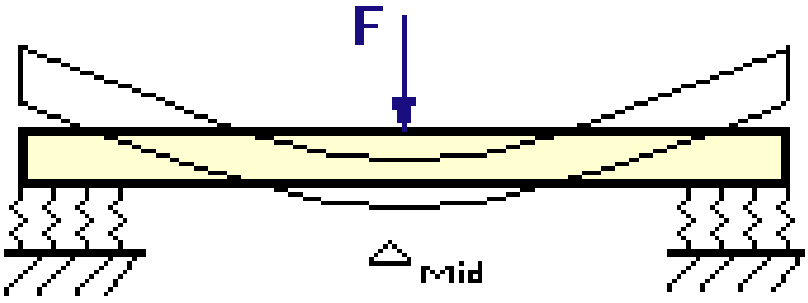

Vita

(May 2003)

Bryan was born on August 12, 1980 in Houston, Texas. After graduating from high school, Bryan entered Texas A&M University in the fall of 1998. He graduated with a B.S. in mechanical engineering in the spring of 2003.

After completing his B.S., he entered the graduate program in Engineering Mechanics at Virginia Polytechnic Institute and State University in the fall of 2003. While at Virginia Tech, he taught ESM 3064, an undergraduate level material's testing laboratory for four semesters. He accepted a full-time mechanical engineering design position in Houston, Texas and begins work on July 12, 2005.